Measurement of Partial Discharges in High Voltage Equipment

by

Yanko Konstantinov Sheiretov

Submitted to the Department of Electrical Engineering and Computer Science
in partial fulfillment of the requirements for the degree of

Bachelor of Science in Electrical Science and Engineering

at the

MASSACHUSETTS INSTITUTE OF TECHNOLOGY

May 1992

© Yanko Konstantinov Sheiretov, MCMXCII. All rights reserved.

The author hereby grants to MIT permission to reproduce and
to distribute copies of this thesis document in whole or in part.

Author . . . .
Department of Electrical Engineering and Computer Science
May 18, 1992

Certified by. . . . .
Dr. Chathan M. Cooke
Principal Research Engineer, Lecturer EECS
Thesis Supervisor

Accepted by . . . .
Leonard A. Gould
Chairman, Department Committee on Undergraduate Theses

Measurement of Partial Discharges in High Voltage Equipment

by

Yanko Konstantinov Sheiretov

Abstract

In this thesis I investigate the possibility of electrically detecting partial discharges in high voltage equipment. Partial discharges are small events that occur in insulation in the presence of high electric field intensity and manifest themselves as pulses of current superimposed on the high voltage lines. They carry important information about the condition and operation of such equipment. Monitoring their characteristic features makes it possible to extract this information. I work on the theoretical design of a system which in response to a current pulse produces a waveform convenient to digitize. In addition I build a physical system based on this model and measure its characteristics. The underlying idea behind this system is adapted from a nuclear physics problem of counting high-energy particles.

Thesis Supervisor: Dr. Chathan M. Cooke
Title: Principal Research Engineer, Lecturer EECS

Contents

List of Figures

List of Tables

Chapter 1

Introduction

The goal of this work is to design a system capable of detecting partial discharges. It must fulfil the requirements set later on in this chapter. The basic structure of the system which will measure partial discharges is as follows: a current sensor is used to produce the initial signal, which is then processed by an analog amplifier/filter. The output of the filter is then processed by a digitizer. The object of the thesis is to select a current sensor and design the analog amplifier/filter. The information needed to make this design possible are the characteristics of the available current sensors and the specifications for the performance of the overall system. This information is presented in this introductory chapter.

Before discussing the specifications on the performance of the overall system, I present some more information on the nature of partial discharges.

1.1 *Partial Discharges*

Partial Discharges (PDs) are small events which occur in insulation in the presence of high electric fields. They constitute a sudden redistribution of charge within, or on the surface of, the insulator. A change in the established pattern of PDs for a particular apparatus can signal change in its operation, which may be due to deterioration, overloading, etc.

PDs produce electrical, acoustic and light emission, each of which may be used for

their detection. The electrical manifestation of PDs is a pulse of current on the line. Typical values for the pulse area are in the picocoulomb range, and for the duration – a few to a few hundred nanoseconds.

The major difficulty with the electrical detection of PDs is the small magnitude of the current pulse as compared to the ambient current and noise on the line, which may be orders of magnitude larger. However, most of the noise energy is in the low frequency range (e.g. 60 Hz), whereas their energy is primarily in the higher frequencies, since PDs are short events. This distinction makes it possible to extract the useful information. In addition to the low-frequency rejection required of the system in order to accomplish this, filtering of specific dominant frequencies (such as 60 Hz) may further reduce the background noise.

There are other methods of measuring PDs, which do not provide on-line real-time results. An example is the volumetric measurement of gas produced by PDs in transformer oil. However, they typically require interruptions of the operation and time delays. This makes the availability of an on-line electrical method very valuable.

1.2   *Specifications*

Depending on the particular application, the importance of the different competing specifications of the system vary. The sensitivity of the system is one of the most important considerations, as it determines the minimum detectable current pulse. The maximum repetition rate is the maximum frequency at which partial discharges may be registered. Since the system response to a pulse of current is a waveform of certain duration, if PDs happen too close in time to each other, the individual responses may interfere and cause errors. There are other restrictions on the waveform, imposed by what kind of wave shapes are convenient to digitize. The system must also be capable of rejecting non-PD signals and external noise. Each of these specifications are discussed in more detail in this section. The requirements for this project imposed by these different specifications are also stated there.

Another characteristic of the system is how it responds to a very large signal at

the input. It is important that it be able to quickly recover from such a large event and not lose its ability to detect partial discharges for too long.

1.2.1 Sensitivity

The sensitivity of the system is characterized by the minimum detectable signal. It has units of charge, i.e. current pulse area. This quantity is determined by the noise characteristics of the system. In order to give a quantitative measure to the sensitivity of the system, I define the minimum detectable signal, (Q_C), to be the amount of charge which will produce a response at the output whose peak value is equal to the RMS value of thermal noise generated in the system.

A signal of this magnitude, of course, will not be detectable at the output, which can be seen from the definition of Q_C. Only a charge a few (maybe ten) times larger than the minimum detectable signal will be visible.

Since most partial discharges are in the picocoulomb range, the system must have a Q_C of $100 - 200fC$ at most, if it is to detect a pulse of one picocoulomb. This is the criterion I use in the design developed in this thesis.

The wave shape of the response also has an effect on the sensitivity. The digitizer measures the first peak of the response. Therefore energy would be wasted in any subsequent peaks. The most efficient waveform from this perspective would be one in which all of the energy is concentrated in the first peak.

1.2.2 Repetition Rate

The response to a partial discharge has a specific duration. This duration determines the minimum period between individual events, for which they would not interfere to cause errors in the measurement.

In order to relate the repetition rate to the dominant time constant of the response, I consider a simple first-order system, whose system function consists of a single pole of time constant τ:

T/τ	2.39	3.04	4.61	9.21
E	0.1	0.05	0.01	0.0001
% Error	10%	5%	1%	0.01%

Table 1.1: Percent Error for Different Repetition Rates

$$F(s) = \frac{1}{1 + \tau s} \tag{1.1}$$

The impulse response of this system is a simple step and decay:

$$f(t) = e^{-\frac{t}{\tau}} \tag{1.2}$$

Assuming that the system is driven by impulses at regular time intervals T, at time $t = 0$ the error of tails accumulated from previous events is:

$$E = e^{-\frac{T}{\tau}} + e^{-\frac{2T}{\tau}} + e^{-\frac{3T}{\tau}} + ... \tag{1.3}$$

This is a geometric progression, whose sum is given by:

$$E = \frac{e^{-\frac{T}{\tau}}}{1 - e^{-\frac{T}{\tau}}} \tag{1.4}$$

Figure 1-1 shows how this error depends on $\frac{T}{\tau}$. Table 1.1 lists a few important points on the graph, which correspond to error values of 10%, 5%, 1% and 0.01%. This data comes to show that a ratio of 5 would make errors negligible. The system must be able to handle repetition rates of at least $100kHz$. For this rate $T = 10\mu s$, i.e. $\tau = 2\mu s$. I shall aim to design a system centered around this time constant.

1.2.3 Digitizer

Since the system is driven by an impulse, the amplitude of the output will be proportional to the area of the current pulse, i.e. to the amount of charge.

In order to make the waveform convenient to digitize, it must fulfil the following requirements:

log Error

1st Order System

T/t
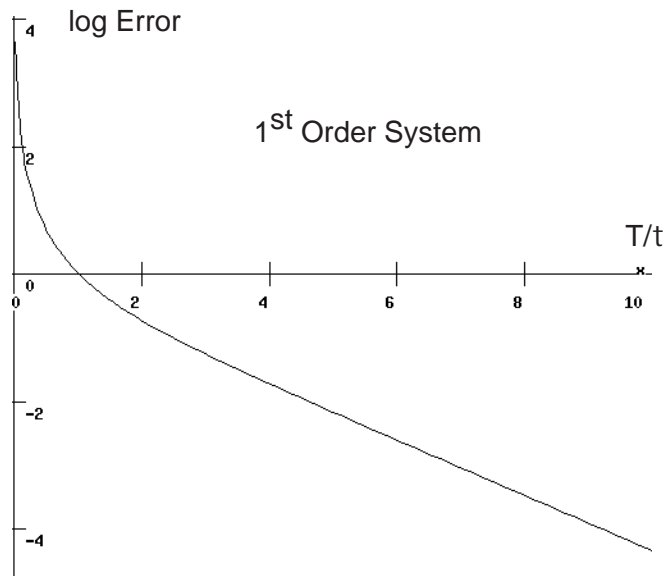
Figure 1-1: Cumulative Error vs Repetition Rate

- The maximum of the output waveform must not occur at, or very close to, its beginning, because of the problem of triggering. If the digitizer triggers on the peak itself, it may not register it properly. This rules out anything that has a step or impulse as part of its response. It is preferable to have a smooth rise.

- The peak must be smooth and wide. Little time should be wasted in what follows the peak, because it yields no useful information. Therefore a waveform with a higher ratio of pulse width to total duration is more suitable. Later in this chapter I give a name to this ratio, 'efficiency', and illustrate its values with examples. This quantity is used to quantify the quality of the waveform.

- The response should integrate to zero, i.e. the total area above and below zero should be the same. The reason for this last requirement is that since the system is linear, any system whose impulse response does not integrate to zero, has at infinity a non-zero step response, and therefore lets DC and low frequencies through. This is very undesirable from the point of view of rejecting

low-frequency noise, as discussed in section 1.1.

The gaussian pulse, discussed in more detail in section 1.3, satisfies the first two requirements quite well. However, since it lies entirely above zero, it is not applicable in this case. Its first derivative is a good choice.

Section 1.3 presents some ideas on how to achieve a system with an 'efficient' impulse response.

1.2.4   Non-PD Signal Rejection (External Noise)

This is noise present on the line together with the PD transients. It may or may not be more significant than the thermal noise. However, ambient power line noise is typically much larger than the PD current pulses, and therefore may need special filtering. In this thesis, I present only a qualitative discussion of external noise, since it is a characteristic of the particular application.

1.2.5   Baseline Restoration

The ORTEC Gaussian amplifiers discussed in the next section have a piece of circuitry whose purpose is to help the system recover form a large input pulse. A similar idea may be employed in this case, but I consider further development of this idea to be beyond the scope of this work.

1.3   *Counting Particles: the ORTEC Equipment*

In their basic nature, the problem of detecting PDs and that of counting high energy particles in Nuclear Physics are very similar. Typically, the latter uses a photomultiplier tube or a semiconductor detector, which respond to a particle with a pulse of charge at its output. It then enters an integrating network at the preamplifier, which responds with a first-order step and decay. When fed to one of the gaussian amplifiers, this signal results in a gaussian pulse at the output. See figure 1-2.
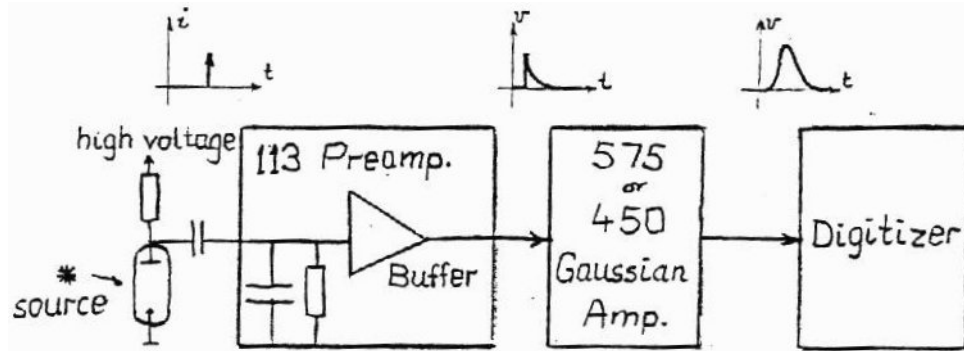
Figure 1-2: Counting Particles in Nuclear Physics

The similarity lies in the fact that both systems respond to a pulse of charge, and the output of both are processed by a digitizer. However, the nature of this pulse of charge is very different. In the Nuclear Physics problem there is no need for low-frequency rejection, since the input is indeed limited to impulses of current and continuous current is absent by the very nature of the source. In the PD problem, on the other hand, continuous current is not only present, but it is much larger than the pulses of interest. Therefore this must be taken in consideration when adapting the transfer function.

1.3.1 The Gaussian Pulse

The gaussian pulse, (or simply "the gaussian"), also known as the bell-shaped curve, has the following mathematical formula:

$$f(t) = e^{-\frac{t^2}{2}} \tag{1.5}$$

Its derivative is:

$$f(t) = -te^{-\frac{t^2}{2}} \tag{1.6}$$
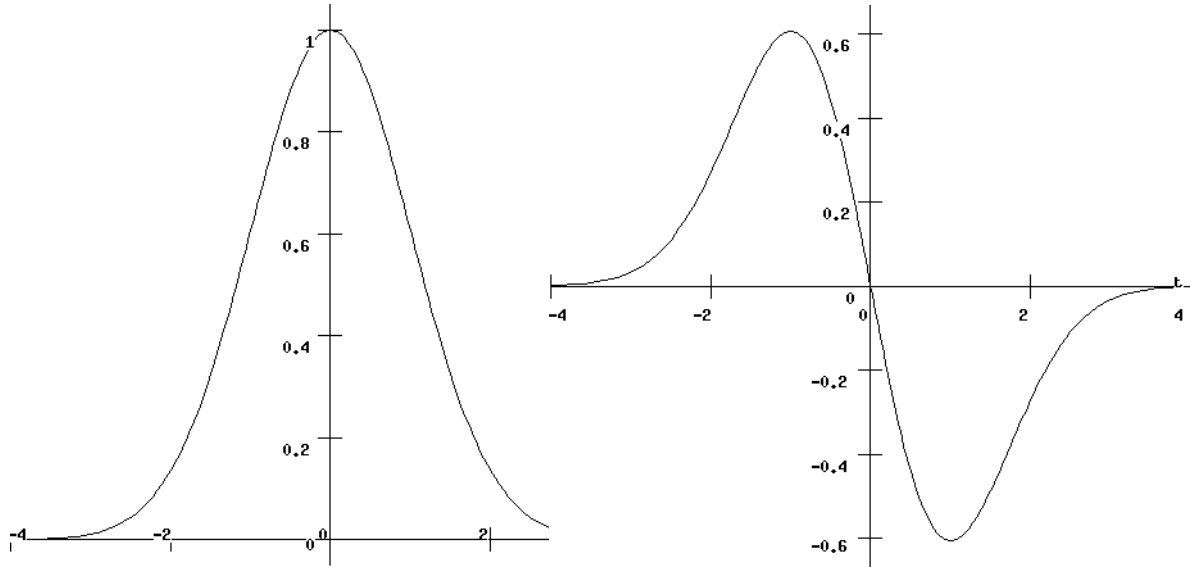
Figure 1-3: The Gaussian Pulse and Its Derivative

Both can be seen on figure 1-3[1].

The Fourier Transform of the gaussian in time is also a gaussian, centered at the origin. This means that a system, whose impulse response is a gaussian[2], has its highest response at DC. As discussed in the previous section, this kind of a system is of no use for PD detection. If the transform of a time-shifted gaussian is still a gaussian (with a linear phase-shift), which function in the time domain would yield a frequency-shifted gaussian in the frequency domain? Such a system would be band-limited, with a very low response at DC. Unfortunately, this is a gaussian-enveloped sinusoid, $e^{-\frac{t^2}{2}}cos(t)$, which is unsuitable.

In the design of the ORTEC equipment, the gaussian-like response was considered desirable because of its good signal-vs-noise characteristics. Unfortunately, the transfer function that implements it, $\frac{1}{(1+\tau s)^n}$, requires that n be infinite, i.e. an infinity of poles. In the ORTEC gaussian amplifiers, the system function used only resembles a true gaussian, but it is implemented with only four poles.

---

[1] The software used to develop this graph is discussed in the appendix

[2] Shifted in time, of course, because the impulse response of a real system must be zero for $t < 0$

16
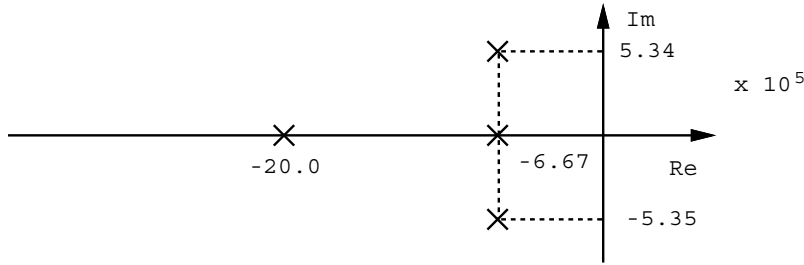
Figure 1-4: PZ-Diagram for the 113/575 Gaussian Amplifier

1.3.2 The ORTEC Gaussian Amplifiers

In this discussion I also include the 113 preamplifier. The output of the photomultiplier tube goes into the 113 preamplifier, before it connects to the gaussian amplifier. The transfer function of the 113 preamplifier has only a single pole and its impulse response is a first order step-and-decay. The gaussian amplifiers use a pole-zero cancellation technique to cancel the pole of the preamplifier and to introduce a new pole at a desired frequency. When referring to the properties of the gaussian amplifiers, I shall refer to the properties of the whole system, including the 113 preamplifier, identified as the 113/575 amplifier.

The 113/575 Amplifier's pole-zero diagram and characteristic responses can be seen on figures 1-4 and 1-5 respectively [3]. Its transfer function is:

$$\frac{V_{out}}{I_{in}} = \frac{K}{(1+\tau s)(1+\frac{\tau}{3}s)(s+\frac{1-0.8j}{\tau})(s+\frac{1+0.8j}{\tau})} \tag{1.7}$$

$$\tau = 0.5, 1.5, 3.0 \mu s$$

One can see that the impulse response of this amplifier very closely resembles a gaussian pulse. The step response on the other hand confirms that this system does not eliminate low frequencies. The model 450 amplifier differs from the 575 only

---

[3]The software used to develop this and subsequent similar graphs is discussed in the appendix
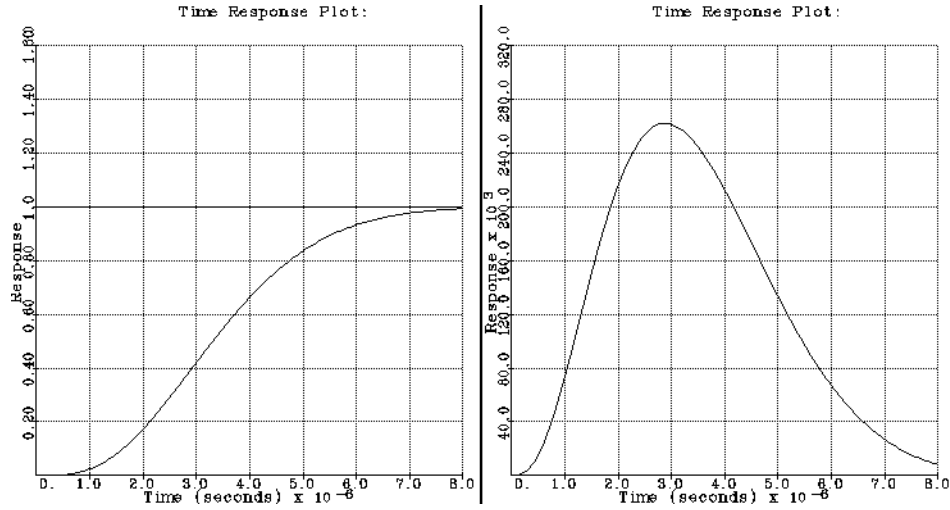
Figure 1-5: Step and Impulse Responses of the 113/575 Gaussian Amplifier

slightly. Its complex pole pair is a little less damped. The design of that amplifier also allows for a wide range of time constants. What is important in this case, however, are the system characteristics, shown in its transfer function:

$$\frac{V_{out}}{I_{in}} = \frac{K}{(1 + \tau s)(1 + \frac{\tau}{3}s)(s + \frac{1-j}{\tau})(s + \frac{1+j}{\tau})} \tag{1.8}$$

As discussed earlier, this transfer function can be used as a model for the development of a PD system, with the introduction of a zero at the origin, i.e. a perfect differentiation, which would introduce low frequency roll-off. Adding the zero is necessary, since it is inherent in the process of current detection and is present in the transfer functions of all current sensors. The low-frequency roll-off also aids in the elimination of ambient $60Hz$.

The pole-zero configuration that may be considered a good choice at this point is the one shown on figure 1-6, with the transfer function shown below. Its step and impulse responses are shown on figure 1-7. They compare well to the true gaussians on figure 1-3.

18
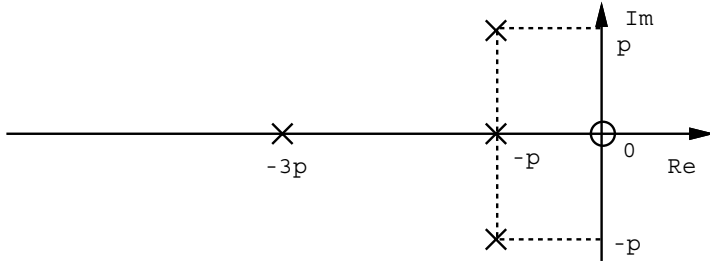
Figure 1-6: Model PZ-Diagram

$$\frac{V_{out}}{I_{in}} = \frac{Ks}{(s+p)(s+3p)[s+p(1-j)][s+p(1+j)]} \tag{1.9}$$

$$p = \frac{1}{\tau}$$

1.3.3 Dependence of the Efficiency on Deviations in the Pole-Zero Configuration

In addition to the visual estimation of the effectiveness of a certain pole position, it is desirable to define a quantitative measure to represent this property. A "good" pole position is one that will give rise to a response, which smoothly rises to its peak value, has a wide peak, and then quickly returns to zero. Thus the following definition of "Efficiency":

$$E = \frac{width}{duration} \tag{1.10}$$

"Duration" is the time period from the beginning of the pulse to the point where it has decreased to e^{-5} or $\approx \frac{1}{150}$ of its peak value. One must remember, that in a sense the efficiency is quite arbitrary in its definition and must not be taken as the sole criterion. "Width" is the time span between the two points on either side of the peak when the value is $\frac{1}{\sqrt{2}}$ of the peak.

In order to get a feel for the range of values E takes on, let us see what the
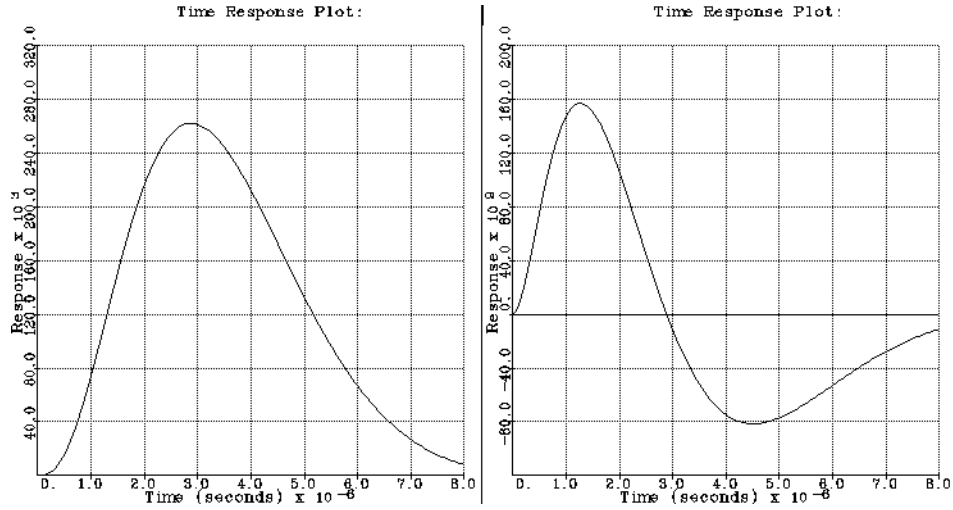
Figure 1-7: Step and Impulse Responses of the Model System

efficiencies of certain known wave shapes are. Following the definitions above, it is easy to find that the efficiency of the gaussian is:

$$E_{GAUSS} = \frac{2 \times \sqrt{ln2}}{2 \times \sqrt{10}} = 0.263$$

This is not as high as some other wave shapes discussed below. This is because although the gaussian quickly returns to zero, it has a slow rise time.

On figure 1-7 one can see that the efficiency of the ideal response developed there is 0.135. It is interesting to find out how deviations from this pole-zero configuration affect the efficiency of the waveform. First I move the central real pole to positions higher and lower. Table 1.2 lists the calculated values of the efficiencies for a few cases. The calculation of the values listed in this table is done numerically with the help of the software outlined in the appendix.

This data is plotted on figure 1-8. It is clear from these calculations that proper positioning of the pole is essential. The reason the efficiency drops quickly with small deviations from the central position is that the system is critically damped for a response of short duration. Moving the pole causes the system to be overdamped or

20

Pole Location	Efficiency with no Zero	Efficiency with a Zero at the Origin
$-0.6p$	0.156	0.095
$-0.8p$	0.217	0.129
$-p$	0.288	0.135
$-1.2p$	0.237	0.115
$-1.4p$	0.225	0.108

Table 1.2: Efficiency vs Central Pole Position

underdamped, leading to a long tail in the former case and ringing in the latter.

I consider moving the fast pole to be not as essential as the central pole, because it is the latter which determined the long-term behaviour. However, another important degree of freedom is the damping ratio of the complex pole pair. It is very clear that lowering the damping ratio will lead to ringing and raising it – to a long tail.

Chapter 3 is dedicated to finding out the most suitable and efficient waveform. It is clear that the highest values of the efficiency occur when the system is critically damped.

1.4 *Current Sensors*

The current sensors I use in this work are coils wound in a way to implement a current transformer with the power line. Specifically, I use current sensors known as Rogowski Coils. The structure of one such coil is shown on figure 1-9. In addition to the winding, these current sensors include lumped elements. There are two different types of such coils available to me: with a resistor and a capacitor in series with the winding, (Series-RC Sensors), and with a resistor and a capacitor in parallel with the winding, (Parallel-RC Sensors).

These two kinds of Rogowski Coils have different circuit models, transfer functions and time-domain responses. In this thesis I take the circuit models as given, and use them to design the subsequent stages of the system.
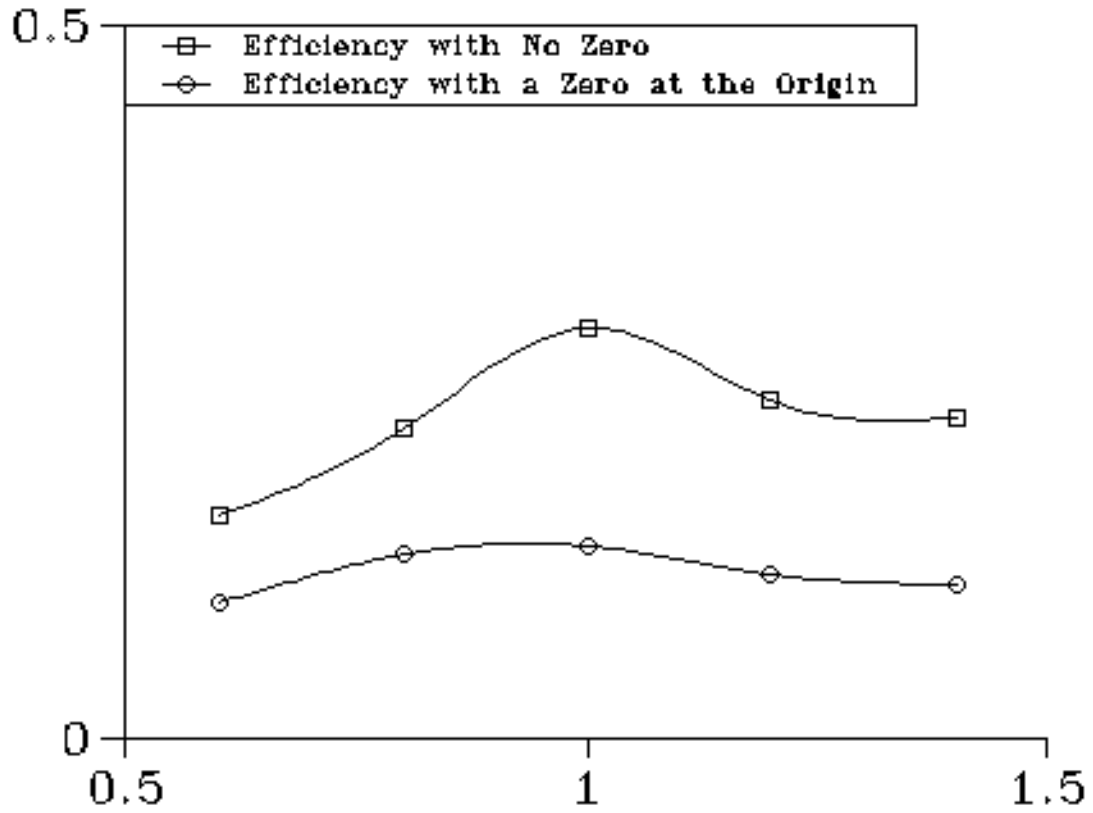
Figure 1-8: Efficiency vs Central Pole Position
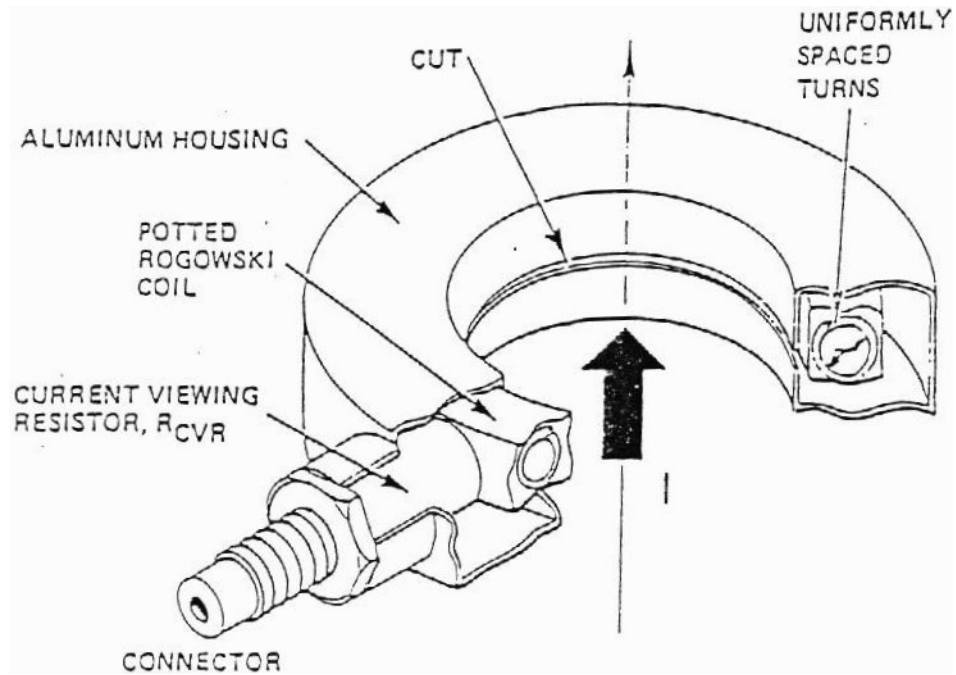
Figure 1-9: Structure of the Rogowski Coils
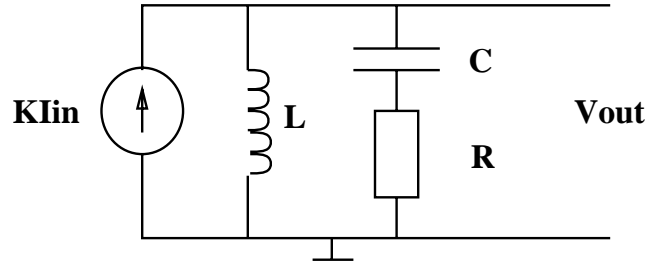
Figure 1-10: Circuit Model for the Series-RC Current Sensors
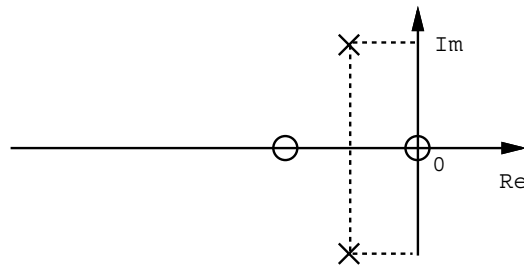
Figure 1-11: Pole-Zero Diagram for the Series-RC Current Sensors

1.4.1 Series-RC Sensors

Figure 1-10 shows the circuit model for this type of sensors, and table 1.3 shows the specific values in the circuit model, characteristic to each type of sensor in this class. Figure 1-11 shows the pole-zero diagram. The system function is:

$$\frac{V_{out}}{I_{in}} = \frac{KRs(s + \frac{1}{RC})}{s^2 + \frac{R}{L}s + \frac{1}{LC}} \tag{1.11}$$

If this transfer function is compared to the model one, equation 1.9, we can see that the zero at the origin is available. The series-RC sensors also have a pair of poles which are complex for the values in table 1.3. This pair of poles can potentially

23

Type	K	L	R	C
PPD-102X	0.33	$33\mu H$	100Ω	$3.6nF$
PPD-103X	0.26	$19\mu H$	58Ω	$6.6nF$
PPD-103XT	0.19	$36\mu H$	100Ω	$3.6nF$

Table 1.3: Circuit Model Values for the Series-RC Sensors
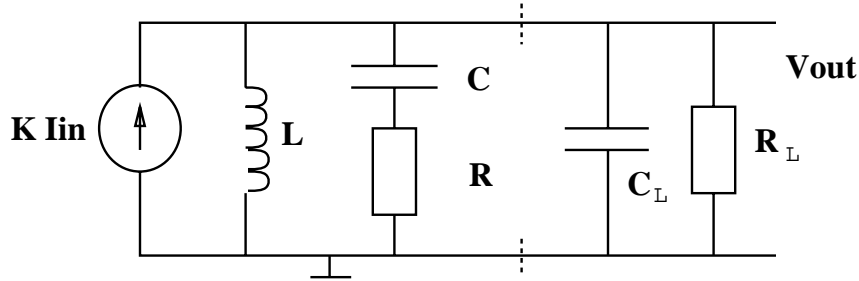
Figure 1-12: Circuit Model of a Loaded Series-RC Sensor

serve as a basis to build the desired system function, because for the available sensors these poles are less damped than required and can therefore be damped to the right amount by external loading. The second zero is not present in the model picture. It is not clear at this stage how it will affect the overall behaviour of the system.

Let us see how the system function changes when this sensor is loaded with a resistance, a capacitance, or both. The new circuit model is shown on figure 1-12. When only a capacitive load is present, $(R_L = \infty)$, the system function is:

$$\frac{V_{out}}{I_{in}} = \frac{K}{C_L} \cdot \frac{s(s + \frac{1}{RC})}{s^3 + (\frac{1}{RC_L} + \frac{1}{RC})s^2 + \frac{1}{LC_L}s + \frac{1}{LRCC_L}} \tag{1.12}$$

A capacitor in parallel adds another real pole at high frequencies and tends to move the complex pair in a way to make it less damped and with a lower natural frequency. When both R_L and C_L are present, the effect of R_L is to damp that complex pole pair. The transfer function becomes:

24
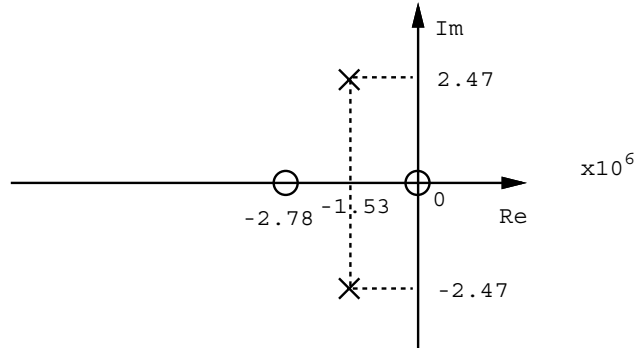
Figure 1-13: Pole-Zero Diagram for the PPD-102X Sensor

$$\frac{V_{out}}{I_{in}} = \frac{K}{C_L} \cdot \frac{s(s + \frac{1}{RC})}{s^3 + (\frac{1}{RC_L} + \frac{1}{RC} + \frac{1}{R_L C_L})s^2 + (\frac{1}{LC_L} + \frac{1}{RR_L CC_L})s + \frac{1}{LRCC_L}} \qquad (1.13)$$

Since the PPD-102X sensor proved to be the most appropriate for the particular application, here I include its characteristics separately. Its pole-zero diagram is shown on figure 1-13 and its step response – on figure 1-14. Figure 1-15 shows an oscilloscope measurement of this step response, which was taken with the setup shown on figure 1-16[4].

1.4.2 Parallel-RC Sensors

Figure 1-17 shows the circuit model for this type of sensors, and table 1.4 shows the specific values in the circuit model, characteristic to each type of sensor in this class. Figure 1-18 shows the pole-zero diagram. The system function is:

$$\frac{V_{out}}{I_{in}} = \frac{K}{C} \cdot \frac{s}{s^2 + \frac{1}{RC}s + \frac{1}{LC}} \qquad (1.14)$$

---

[4]More about the hardware used may be found in the appendix
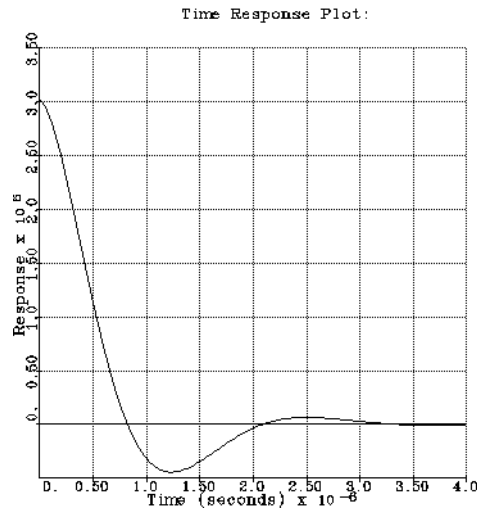
Figure 1-14: Calculated Unloaded Step Response of the PPD-102X Sensor
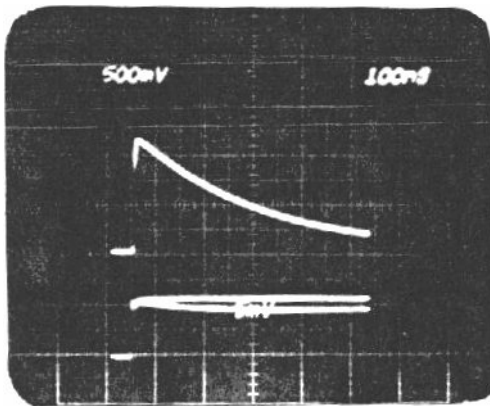
Trace	Description	Units
Top	Output (unloaded)	$100mV/smdiv$
Bottom	Unused	
Sweep		$200ns/smdiv$

Figure 1-15: Measured Unloaded Step Response of the PPD-102X Sensor

Type	K	L	R	C
PPD-101X	0.023	$7.5mH$	840Ω	$150pF$
PPD-101	0.025	$1.3mH$	420Ω	$150pF$
PPD-101BT	0.022	$3.0mH$	725Ω	$170pF$
PPD-100B	0.022	$1.1mH$	730Ω	$160pF$

Table 1.4: Circuit Model Values for the Parallel-RC Sensors

26
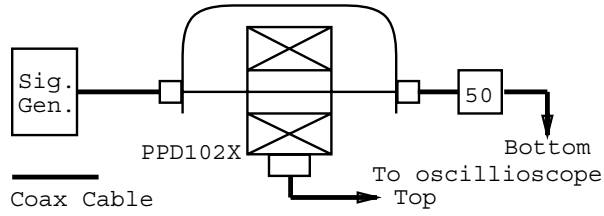
Figure 1-16: Experimental Setup for the Measurement on Figure 1-15
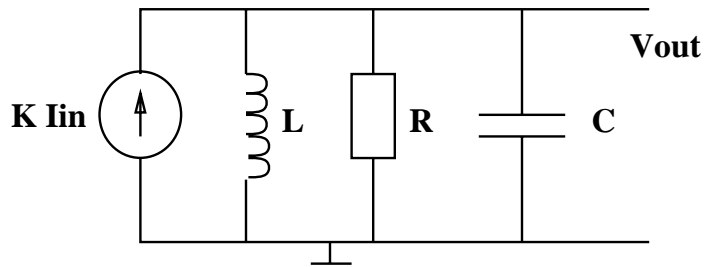
Figure 1-17: Circuit Model for the Parallel-RC Current Sensors
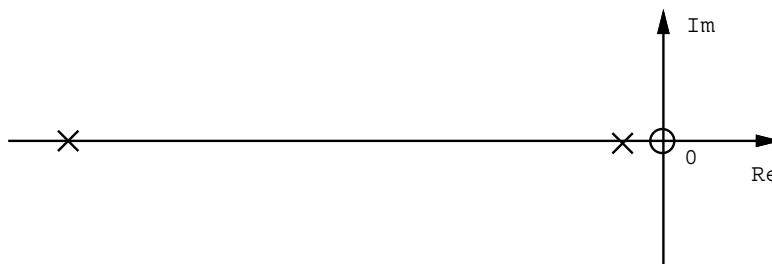
Figure 1-18: Pole-Zero Diagram for the Parallel-RC Current Sensors
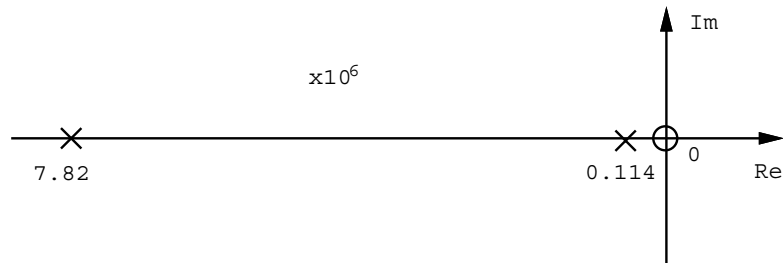
Figure 1-19: Pole-Zero Diagram for the PPD-101X Sensor

This kind of current sensors' pole-zero configuration can be used as a basis in the building of the model system too. For the values shown in table 1.4, the damping ratio of the two poles is greater than one. We could have the model PZ-configuration be centered around the slower pole. The zero at the origin falls in with the model, and in this case there is no other zero to consider.

Because of their parallel structure, any kind of capacitive or resistive loading simply adds to their characteristic values. This kind of loading would not change the character of the transfer function, only its parameters.

Figure 1-19 shows the pole-zero diagram of a typical representative of this type of sensors – PPD101X. Its calculated step response is shown on figure 1-20 and the oscilloscope measurement, taken with the same setup as the response of PPD102X, on figure 1-21.

These are the resources available to me in the development of this thesis work. The information presented in this introductory chapter, and in particular the circuit models and the circuit model values for the current sensors, is taken as given. The following chapters do not discuss or research the validity of these models.
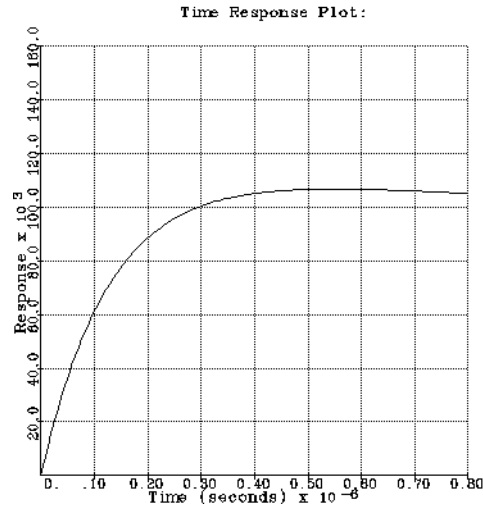
Figure 1-20: Calculated Unloaded Step Response of the PPD-101X Sensor
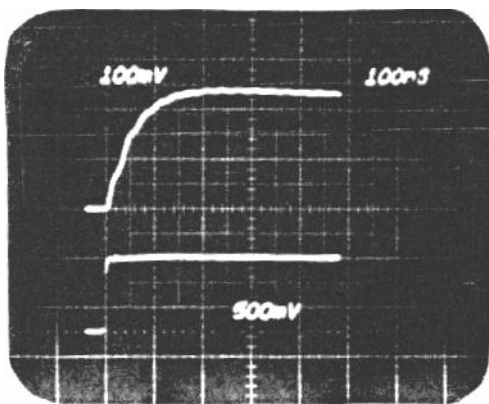
Trace	Description	Units
Top	Output (unloaded)	$100mV/smdiv$
Bottom	Drive into 50Ω	$500mV/smdiv$
Sweep		$100ns/smdiv$

Figure 1-21: Measured Unloaded Step Response of the PPD-102X Sensor

29

Chapter 2

Thermal Noise Limits

The most important consideration in doing the design at the front end of the system is minimizing the thermal noise generated by resistors before the first gain stage. Such resistors are present in both kinds of current sensors. The amount of thermal noise at the output of the system depends on the value of the noisy resistor, on the bandwidth of the system and on its gain within this bandwidth. The last two factors are affected by the size of the integrating capacitors, by the size of the load impedance of the sensor, etc. All of these factors are interrelated in a way that would require more detailed analysis to establish the best strategy at hand.

In general, we would like to capture as much of the energy of the pulse as possible. The pulse of current on the line generates a pulse of current in the current source in the circuit model of the sensor. Unless there is a capacitance in parallel with the winding to integrate the impulse of current to a step of voltage, the voltage output of the sensor will be dominated by an impulse of voltage, as it appears across the resistance. (See figures 1-10 and 1-17.) Since the gain stage loading the sensor is an active circuit, it's band-limited, and therefore will lose some of the energy of this voltage pulse, due to saturation and limited rise time.

If, on the other hand, a load capacitance is present, the impulse of current will generate a step of voltage across this capacitance, and much more of the energy of the pulse will be captured by the active circuit. This is the argument behind the need for a load capacitance. The parallel-RC sensors already have such capacitance, but

the other kind don't.

2.1   *Integration*

The load capacitance discussed above acts as an integration. Even if there is no load capacitance, integration is necessary in order to achieve the model transfer function, no matter which kind of sensor is used. Integration tends to limit the bandwidth at the high frequency end.

For a first-order RC-network, which consists of a resistor (R) and a capacitor (C), the RMS value of the noise depends only on the capacitance, as can be seen in the formula below:

$$v_{RMS}^2 = 4kTR\Delta f = 4kTR\frac{1}{2\pi RC} = \frac{2kT}{\pi C} \tag{2.1}$$

$$
\begin{aligned}
k &= 1.38 \times 10^{-23}[J/K] \quad &\text{Boltzman's constant} \\
T&[K] \quad &\text{Absolute temperature} \\
\Delta f&[Hz] \quad &\text{Bandwidth}
\end{aligned}
$$

Does it make a difference then whether we integrate before or after the first gain stage? This is a reasonable question, because integration after the first gain stage allows us to use a different resistance, whose thermal noise would not be significant, since it is after the gain. In other words, does this additional degree of freedom allow us to control the bandwidth and the signal-to-noise ratio independently? This is the question which this section answers.

First let us consider a system based on a series-RC sensor, loaded with a capacitance and a noiseless resistance (the input impedance of an active stage). The thermal noise source is represented by a voltage source in series with the noisy resistor. The circuit diagram may be seen on figure 2-1. This system is characterized by its two transfer functions: signal and noise (see equation 1.13):
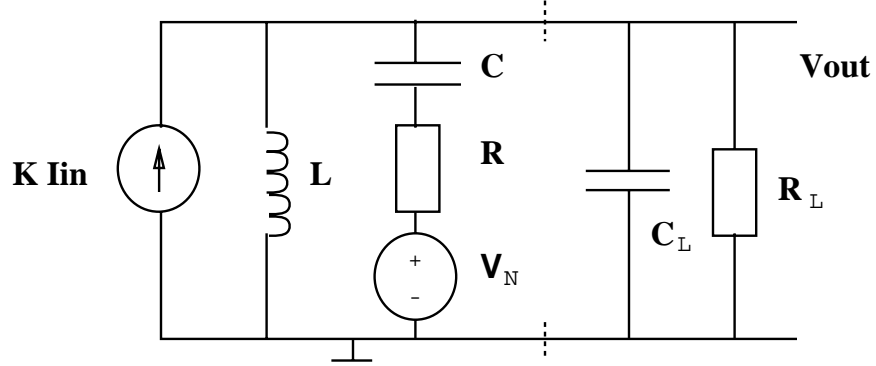
Figure 2-1: Circuit Diagram of a System Based on a Series-RC Sensor

$$\frac{V_{out}}{I_{in}} = \frac{K}{C_L} \cdot \frac{s(s + \frac{1}{RC})}{s^3 + (\frac{1}{RC_L} + \frac{1}{RC} + \frac{1}{R_L C_L})s^2 + (\frac{1}{LC_L} + \frac{1}{RR_L CC_L})s + \frac{1}{LRCC_L}} \qquad (2.2)$$

$$\frac{V_{out}}{V_N} = \frac{1}{RC_L} \cdot \frac{s^2}{s^3 + (\frac{1}{RC_L} + \frac{1}{RC} + \frac{1}{R_L C_L})s^2 + (\frac{1}{LC_L} + \frac{1}{RR_L CC_L})s + \frac{1}{LRCC_L}} \qquad (2.3)$$

When comparing these two transfer functions, there are a few important features to notice: since it is a linear system, the two transfer functions have identical sets of poles; the zeros of the transfer functions do not depend on the value (or on the very presence) of C_L; the Bode (DC) gains of the two functions have the same dependence on C_L.

Now suppose that we build a hypothetical system, which has no C_L at the front end, but which has **exactly the same** signal transfer function, in which the extra pole needed is added at a subsequent filter stage. This hypothetical system will have values of R and C identical with the prototype, so that the noise generation and the position of the zero are not changed. It is possible to create it, because L and R_L give us the two degrees of freedom necessary to move the two poles of the hypothetical

system to coincide with the poles of the C_L-loaded prototype, and additional filtering after the first gain (buffer) stage will help match the transfer function.

The question is, what is the noise transfer function and generation of this hypothetical system, as compared to the prototype, and is there any advantage to the new scheme? The answer is that this hypothetical system will have exactly the same noise picture, because:

- $v_{N,RMS}^2$ depends only on R and Δf. By the definition of the hypothetical system, both of these are identical.

- The zeros of the two transfer functions do not move with C_L, whereas the poles are the same, since the signal and the noise transfer functions always have the same set of poles. This means that the noise transfer function of the hypothetical system has the same pole-zero configuration as that of the original system.

- The Bode gain coefficients of the two types of transfer functions have the same dependence on C_L. This means that if the two signal transfer functions have the same value (by definition), then the two noise transfer functions have the same Bode gain too.

This means that the two noise transfer functions are the same and the noise source is the same, i.e. there is no advantage to integrating after the first gain stage.

Since the zeros and the Bode gains do not depend on R_L, one may use the same arguments as presented above to conclude that the level of thermal noise generated in the current sensor does not depend on the load impedance, if the same overall transfer function is used. The load impedance itself is a source of noise, but it represents noise generated in the active amplifier and is not part of the front-end design.

On the other hand, if we compare the Bode gains of the signal and the noise transfer functions, it becomes clear that a larger R proportionately increases the useful signal, as compared to the noise. The RMS value of the noise source also increases with R, but only as its square root. This means that if we had control
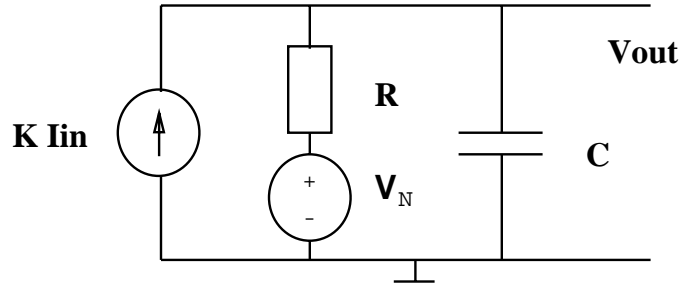
Figure 2-2: First-Order RC System Circuit Diagram

over the value of R, we would like it to be as large as possible. This conclusion was intuitively obvious from the beginning, since a noiseless system would include no resistance at the front end. If we were to design a current sensor with a high sensitivity, we would use only a winding with a capacitance in parallel. The damping of this LC-system would be controlled by the load impedance. This kind of a system would have no thermal noise generated at the front end, and would consequently have a much higher sensitivity.

2.2 *Bandwidth*

It would be interesting to see how integration, characterized by its bandwidth, affects the signal-to-noise ratio. Let us first consider a simple example of a first-order RC system and see what affects this ratio and how. The circuit diagram for this example is shown on figure 2-2. The diagram shows both the signal source, (a current source), and the noise source, (a voltage source in series with the noisy resistor).

The signal transfer function is:

$$\frac{V_{out}}{I_{in}} = \frac{K}{C} \cdot \frac{1}{s + \frac{1}{RC}} \tag{2.4}$$

In order to calculate the voltage output for a current pulse of unit area, (1 Coulomb), we must take the inverse Laplace transform of equation 2.4, which is:

$$v(t) = \frac{K}{C} e^{-\frac{t}{RC}} \tag{2.5}$$

The maximum occurs at $t = 0$, therefore

$$\frac{V_{max}}{Q} = \frac{K}{C} \tag{2.6}$$

Now let us consider the noise transfer function. It is

$$\frac{V_{out}}{V_N} = \frac{1}{RC} \cdot \frac{1}{s + \frac{1}{RC}} \tag{2.7}$$

$$v_{N,RMS}^2 = 4kTR\Delta f \tag{2.8}$$

$$\Delta f = \frac{1}{2\pi RC} \tag{2.9}$$

From equation 2.7 we can see that at low frequencies $\frac{V_{out}}{V_N} = 1$. Then the above relationships yield that the noise is independent of R and inverse with the square root of C;

$$v_{out,RMS} = \sqrt{4kTR\frac{1}{2\pi RC}} = \frac{\sqrt{\frac{2}{\pi}kT}}{\sqrt{C}} \tag{2.10}$$

Minimum Detectable Signal (MDS), Q_C, to be the amount of charge (current pulse area) which would produce a voltage waveform with a maximum value equal to the RMS value of the thermal noise. For the simple system discussed above, we can make the voltages in equations 2.6 and 2.10 equal in order to calculate the MDS:

$$Q_C = \frac{C}{K} \cdot \frac{\sqrt{\frac{2}{\pi}kT}}{\sqrt{C}} = \frac{\sqrt{\frac{2}{\pi}kT}}{K} \cdot \sqrt{C} \tag{2.11}$$

The lower the MDS, the greater the sensitivity of the system. Therefore, lower C means higher sensitivity. To express this relationship in terms of the bandwidth, we can use equation 2.9, to obtain
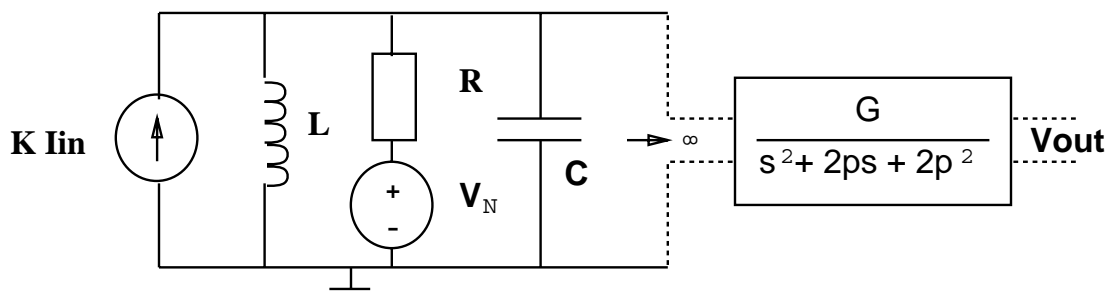
Figure 2-3: More Complex System Circuit Diagram

$$Q_C = \frac{\sqrt{\frac{2}{\pi}kT}}{K} \cdot \frac{1}{\sqrt{R2\pi\Delta f}} = \frac{1}{\pi K} \cdot \frac{\sqrt{kT}}{\sqrt{R\Delta f}} \tag{2.12}$$

This means that for this simple example the relationship $Q_C \propto \frac{1}{\sqrt{\Delta f}}$ holds. I believe that the same relationship holds for any system with a similar structure at the front end, i.e. the faster the system, the more sensitive it is. In order to confirm this claim, let us consider another example of a system based on the structure of one of the current sensors. The circuit diagram is shown on figure 2-3. A parallel-RC current sensor is loaded with a filter/amplifier of infinite input impedance. For simplicity, I have assumed that the values of the sensor elements are such that the real poles of its PZ configuration are a factor of 3 apart. (See figure 2-4.) The other two complex poles on that figure are contributed by the amplifier/filter, whose transfer function is shown below:

$$\frac{V_{out}}{V_{in}} = \frac{G}{s^2 + 2\zeta\omega_n s + \omega_n^2} = \frac{G}{s^2 + 2ps + 2p^2} \tag{2.13}$$

$$\zeta = \frac{1}{\sqrt{2}} \qquad\qquad \omega_n = \sqrt{2}p$$

In this transfer function p is a parameter defined on figure 2-4. The pole-zero configuration shown on that figure is the one shown on figure 1-6. The bandwidth of this system is now characterized by the parameter p.

The signal and noise transfer functions of the system respectively are:

36
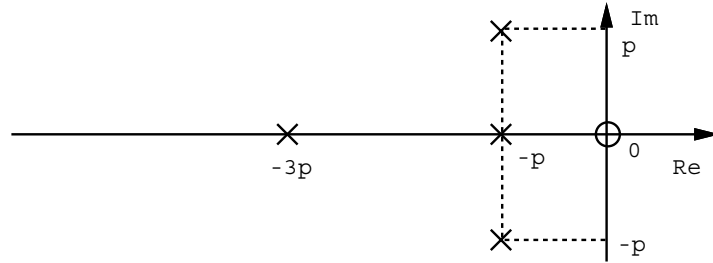
Figure 2-4: More Complex System Pole-Zero Diagram

$$\frac{V_{out}}{I_{in}} = \frac{KG}{C} \cdot \frac{s}{(s+p)(s+3p)(s^2+2ps+2p^2)} \tag{2.14}$$

and

$$\frac{V_{out}}{V_N} = \frac{G}{RC} \cdot \frac{s}{(s+p)(s+3p)(s^2+2ps+2p^2)} \tag{2.15}$$

First, let us calculate the maximum voltage per unit charge. To do that, we need to take the inverse Laplace transform of equation 2.14. It can be broken up using partial fractions.

$$\frac{V_{out}}{I_{in}} = \frac{KG}{C}\left(\frac{-\frac{1}{2p^2}}{s+p} + \frac{\frac{3}{10p^2}}{s+3p} + \frac{\frac{1}{5p^2}s + \frac{4}{5p}}{s^2+2ps+2p^2}\right) \tag{2.16}$$

$$v(t) = \frac{KG}{C}\left[-\frac{1}{2p^2}e^{-pt} + \frac{3}{10p^2}e^{-3pt} + \frac{\sqrt{10}}{5p^2}e^{-pt}sin(pt+\phi)\right] \tag{2.17}$$

$$\phi = 18.4^o$$

In order to locate the maximum of this waveform we must set its derivative to zero. This leads to the following transcendental equation:

$$\frac{p}{2p^2}e^{-pt} - \frac{9p}{10p^2}e^{-3pt} + \frac{\sqrt{10}}{5p^2}[-pe^{-pt}sin(pt+\phi) + pe^{-pt}cos(pt+\phi)] = 0 \qquad (2.18)$$

This equation simplifies to:

$$\frac{1}{2} - \frac{9}{10}e^{-2pt} + \frac{\sqrt{10}}{5}[-sin(pt+\phi) + cos(pt+\phi)] = 0 \qquad (2.19)$$

This equation will have a solution in terms of pt, i.e. $pt = [const.]$. This means that when the value for t is substituted in equation 2.17, the latter will take the form:

$$V_{max} = \frac{KG}{Cp^2}[constant] \qquad (2.20)$$

or

$$V_{max} \propto \frac{1}{Cp^2} \qquad (2.21)$$

Of course, the gain of the amplifier/filter is not independent of p and therefore the equation above cannot be used to determine how the maximum voltage depends on the bandwidth. This equation is useful only to determine the **relative** effect of p, characterized by the MDS.

In that last formula, C and p are not independent. The current sensor is characterized by three values, which govern its frequency characteristics: R, C and L. Since thermal noise depends on R, and we are trying to estimate the effect of the bandwidth only, R must be kept constant. We therefore have two degrees of freedom, C and L, to satisfy two constraints: the two poles at $-p$ and $-3p$. This means that for a given R, the parameter p completely determines C. From equations 2.14 and 2.15 one can see that the characteristic equation of the current sensor is

$$s^2 + 4ps + 3p^2 = 0 \qquad (2.22)$$

If we match this equation to equation 1.14, we get:

38

$$\frac{1}{p^2} = 3LC \qquad\qquad \frac{L}{C} = \frac{16R^2}{3}$$

$$C = \frac{1}{p4R}$$

When we substitute this last relationship into equation 2.21, we get:

$$V_{max} \propto C \propto \frac{1}{p} \tag{2.23}$$

Now let us look at how noise is affected by p. The bandwidth is proportional to p. For simplicity I shall assume that:

$$\Delta f = \frac{p}{2\pi} \tag{2.24}$$

When the magnitude of the transfer function 2.15 is evaluated at $s = jp$, we get:

$$\left| \frac{jp}{(jp + p)(jp + 3p)(-p^2 + 2jp^2 + 2p^2)} \right| \propto \frac{1}{p^3} \tag{2.25}$$

When all relationships, 2.15, 2.24, and 2.25, are considered, we get:

$$v_{out,RMS} \propto \frac{1}{C} \cdot \frac{1}{p^3} \cdot \sqrt{\Delta f} \propto \frac{1}{p^{3/2}} \tag{2.26}$$

This, combined with equation 2.23 to eliminate C, gives us the relationship which was expected:

$$Q_C \propto \frac{1}{\sqrt{p}} \propto \frac{1}{\sqrt{\Delta f}} \tag{2.27}$$

The conclusion that must be drawn from these two examples, is that for a fixed R at the front end, the signal-to-noise ratio is better for a faster system, with a proportionality relationship as shown on equation 2.27. This seems counterintuitive, since thermal noise increases with a wider bandwidth. However, in this application the signal-to-noise ratio is higher for a faster system, because the output voltage is inversely proportional to the integrating capacitance, (i.e. directly proportional to

the bandwidth), whereas the RMS value of the noise increases only with the square root of the bandwidth.

Of course there are other limitations on the speed of the system, such as the requirements of the digitizer and they must be considered too when the speed of the response is determined.

2.3 *Capacitive Loading*

In the two previous sections I showed that a system's signal-to-noise ratio depends only on the bandwidth and on the transformer ratio K, (if the noise-generating resistor R is kept constant), and if these are kept constant, the details of the system implementation are not important. Suppose we have a series-RC sensor with a load capacitance C_L. Even when $C_L = 0$ the sensor has a limited bandwidth. In this chapter I will find the maximum value of C_L which would not significantly slow down the system.

The characteristic equation of this system is

$$(s + p)(s^2 + 2\zeta\omega_n s + \omega_n^2) = s^3 + (p + 2\zeta\omega_n)s^2 + (\omega_n^2 + 2\zeta\omega_n p)s + p\omega_n^2 = 0 \quad (2.28)$$

where p here is the real pole, and ζ and ω_n are the damping ratio and natural frequency of the complex pair. If C_L is small (compared to C), then

$$p \approx \frac{1}{(R_L \parallel R)C_L} \qquad\qquad p \approx \frac{R_L + R}{R_L R C_L} \qquad\qquad (2.29)$$

If equations 1.13 and 2.28 are compared, we can see that

$$p\omega_n^2 = \frac{1}{RCC_L L} \qquad\qquad \omega_n^2 = \frac{R_L}{R_L + R} \cdot \frac{1}{LC} \qquad\qquad (2.30)$$

At this approximation, C_L does not affect ω_n, i.e. the bandwidth. To see exactly how large C_L can get before it significantly reduces the speed of the response, we must tabulate some values for a specific example.

C_L, pF	Complex Pair, $10^6 s^{-1}$	ζ	Real Pole, $10^6 s^{-1}$
0	$1.43 \pm 0.87j$	0.854	∞
100	$1.43 \pm 0.87j$	0.854	299
200	$1.42 \pm 0.89j$	0.847	150
300	$1.41 \pm 0.90j$	0.843	100
510	$1.40 \pm 0.91j$	0.838	58.8
820	$1.40 \pm 0.93j$	0.833	36.6
1000	$1.38 \pm 0.94j$	0.826	30.0
1500	$1.35 \pm 0.98j$	0.810	20.1
2200	$1.32 \pm 1.03j$	0.788	13.8
2600	$1.29 \pm 1.05j$	0.776	11.7
3300	$1.24 \pm 1.09j$	0.751	9.43
4700	$1.14 \pm 1.14j$	0.707	6.88
5100	$1.10 \pm 1.16j$	0.688	6.45
7100	$0.96 \pm 1.19j$	0.628	5.08
10000	$0.78 \pm 1.20j$	0.551	4.22

Table 2.1: Dependence of PPD-102X Poles on the Load Capacitance

Out of all current sensors, I chose PPD-102X (see table 1.3), because it has the highest value of K. A parallel-RC sensor typically would have a larger value for R, which means a better signal-to-noise ratio, but these sensors also give rise to much slower systems, and I believe on the whole PPD-102X would give rise to the most sensitive system. In order to be certain of that, a theoretical system must be developed based on a parallel-RC sensor, and then the two systems must be compared.

Consider the sensor PPD-102X, with circuit model values as shown in table 1.3, loaded with 50Ω of active stage input impedance, and C_L. Table 2.1 shows how the complex pole pair, its damping ratio ζ, and the real pole, vary with C_L. The data in this table is plotted on figure 2-5. Logarithmic scale is used on all axes except the damping ratio. One can see on this figure that the approximation used in equation 2.29 is still valid for values of C_L up to $7100pF$.

Since the signal-to-noise ratio has a square-root dependence on the bandwidth, a 20% and a 10% deterioration of the bandwidth causes a 10% and a 5% deterioration of the signal-to-noise ratio. The dependence of the latter on the load capacitance is shown on figure 2-6. The 20% and 10% points are shown on figure 2-5 and they
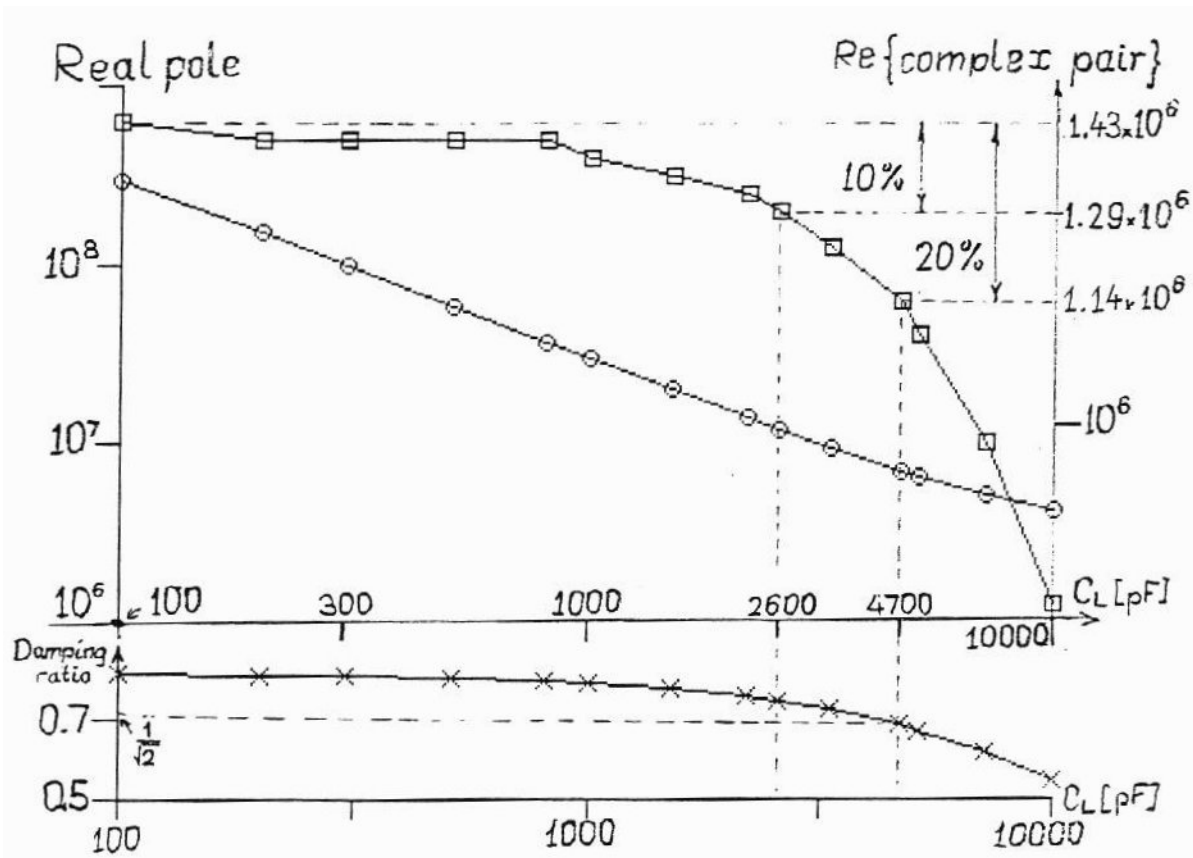
Figure 2-5: Dependence of PPD-102X Poles on the Load Capacitance
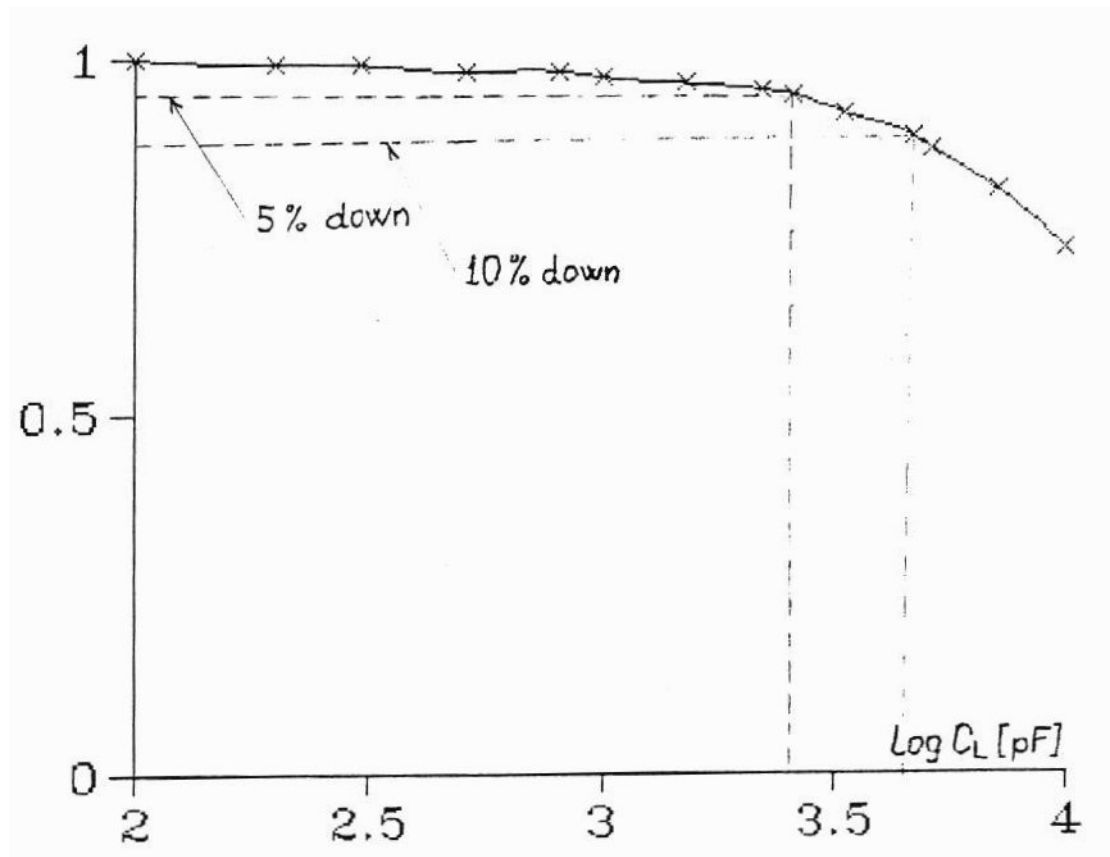
Figure 2-6: Dependence of the Signal-to-Noise Ratio on the Load Capacitance

correspond to $4700pF$ and $2600pF$ of C_L respectively. It is interesting to note that for $C_L = 4700pF$ the damping ratio is $\frac{1}{\sqrt{2}}$, exactly as in the 450 Gaussian Amplifier. This value corresponds to a 10% decrease of the signal-to-noise ratio. For these reasons it is reasonable to take this value as the optimal choice for a loading capacitor.

The pole-zero configuration of the PPD-102X sensor, loaded with a $4700pF$ capacitor and input impedance of 50Ω is shown on figure 2-7. This will be used in the next chapter as the basic front-end response. The amplifier/filter will accommodate the existing pole-zero configuration to the most desirable system function.

A calculation of the minimum detectable signal of the so designed system is carried out in Chapter 4, when the transfer function of the total system, including the filter, is known.
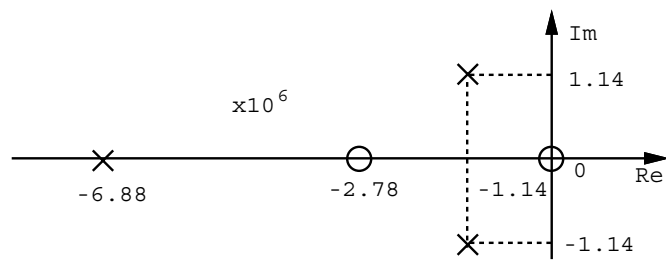
Figure 2-7: Pole-Zero diagram of PPD-102X Loaded with $4700pF$ and 50Ω

Chapter 3

Waveform Shaping

The next stage in the development of the system is the amplifier. Everything that happens at and after the first gain stage falls in this category. Thermal noise is not a factor in this discussion, since thermal noise at the output is dominated by that generated before the first preamplifier stage. The amplifier/filter stage can therefore be fully described by its system function and Bode gain.

At this stage I shall take the front-end structure, developed in the previous chapter, as given, and use its mathematical representation to design an appropriate system function for the amplifier. Figures 1-6 and 1-7 show one good transfer function. However, the system function of the current sensor, shown on figure 2-7, is significantly different. It has an extra pole, an extra zero and lacks two real poles. In principle, the zero could be cancelled first, but it is not clear at this point whether this is really necessary. Since poles are easy to implement, I suggest a different strategy, which entails adding a pole first and finding its most appropriate position. The latter is found by using a numerical method [1] to calculate the impulse response and investigating its characteristics. In this way the possibility of cancelling the zero is not eliminated, as the pole may be placed at the same location.

---

[1]See appendix.
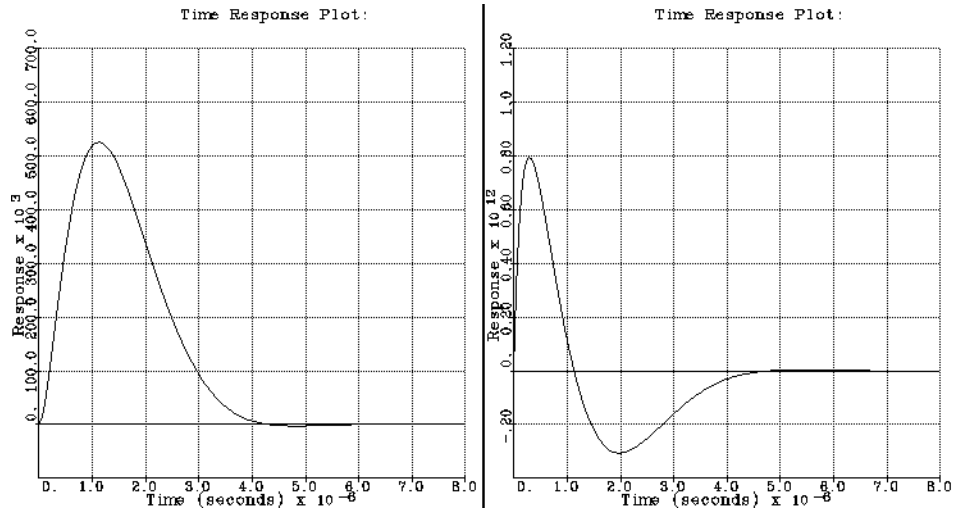
Figure 3-1: Step and Impulse Responses with a Pole at -1.2×10^6: Underdamped

3.1   *First Pole*

Figure 2-7 shows the pole-zero configuration that is used as the basis for this calculation. By adding one more pole I am trying to find the configuration that will result in the highest efficiency.

Let us start with a pole slightly faster than the real part of the complex pair. The response, shown on figure 3-1, is clearly underdamped. We are looking for a critically damped response, since it will last shorter. When the pole is positioned right in between the complex pole pair, the response is still underdamped (figure 3-2). Figures 3-3, 3-4, and 3-5 show one more underdamped and two overdamped responses, for various positions of the pole. (See figure captions.)

It turns out that critical damping occurs with the pole at -1.05×10^6. The response may be seen on figure 3-6. Figure 3-7 shows the impulse response of this system on a different time scale, which makes reading off the graph of the parameters needed in the calculation of the efficiency of this configuration easier.

This is the best solution with a single pole. The efficiency of this network is $E = 0.108$, which is relatively low in comparison to the number characteristic of the
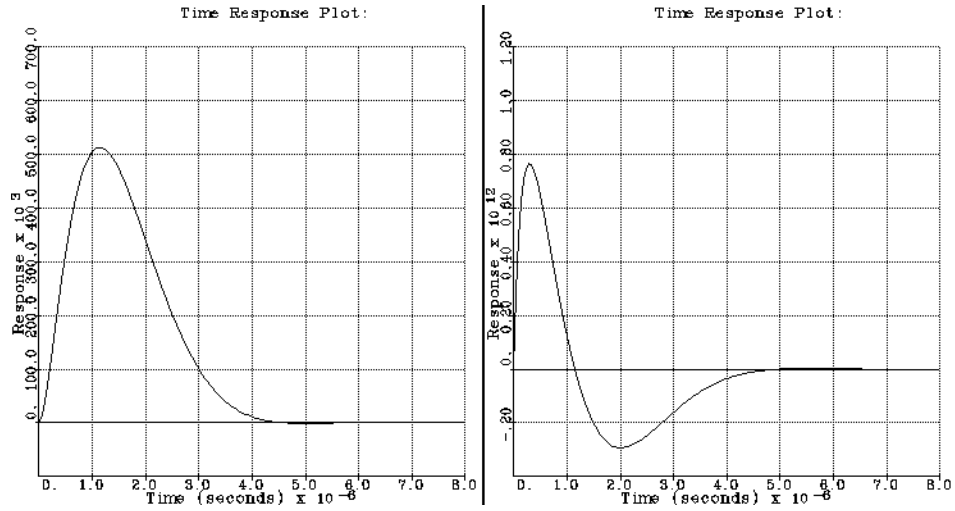
Figure 3-2: Pole at -1.14×10^6: Underdamped
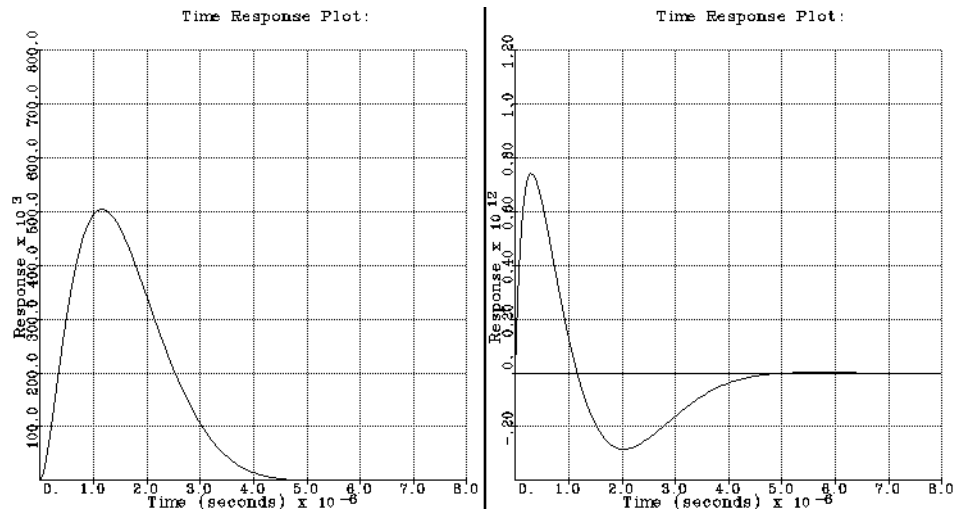
Figure 3-3: Pole at -1.10×10^6: Underdamped
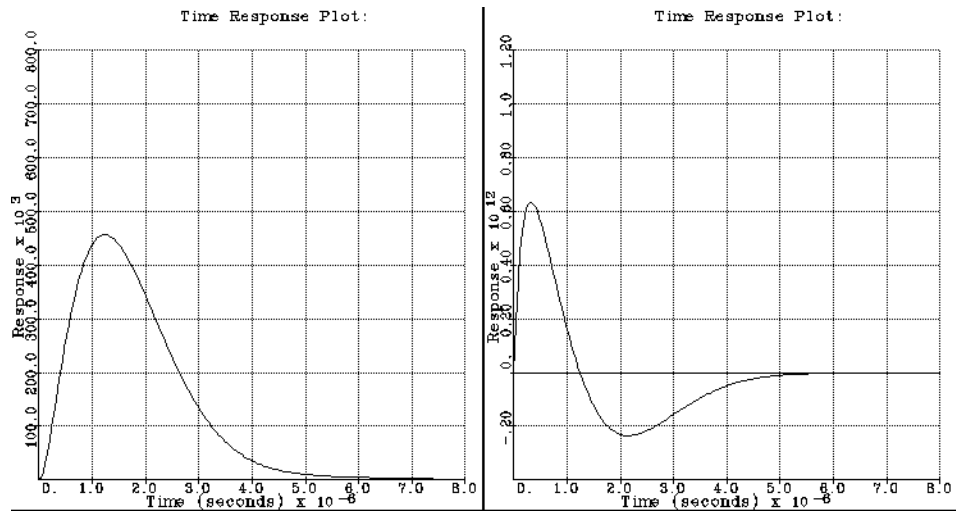
Figure 3-4: Pole at -0.9×10^6: Overdamped
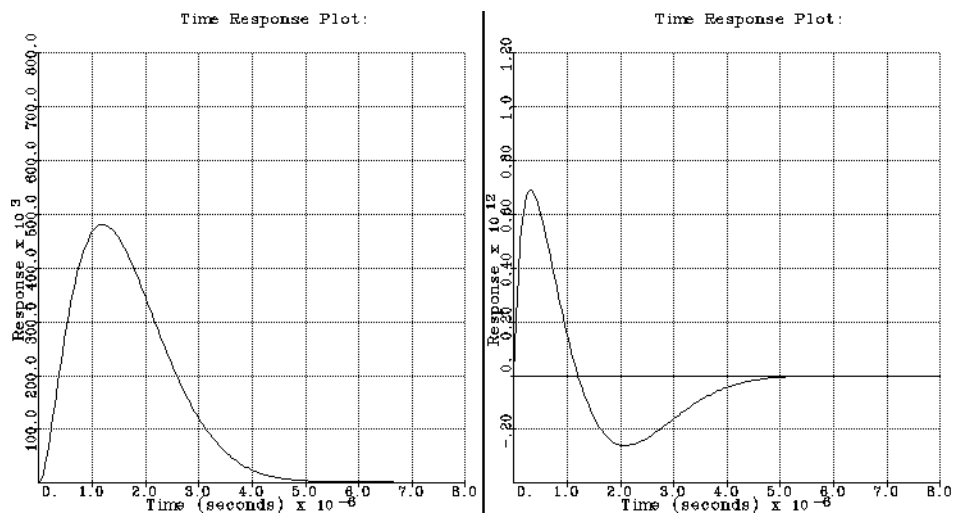
Figure 3-5: Pole at -1.00×10^6: Overdamped
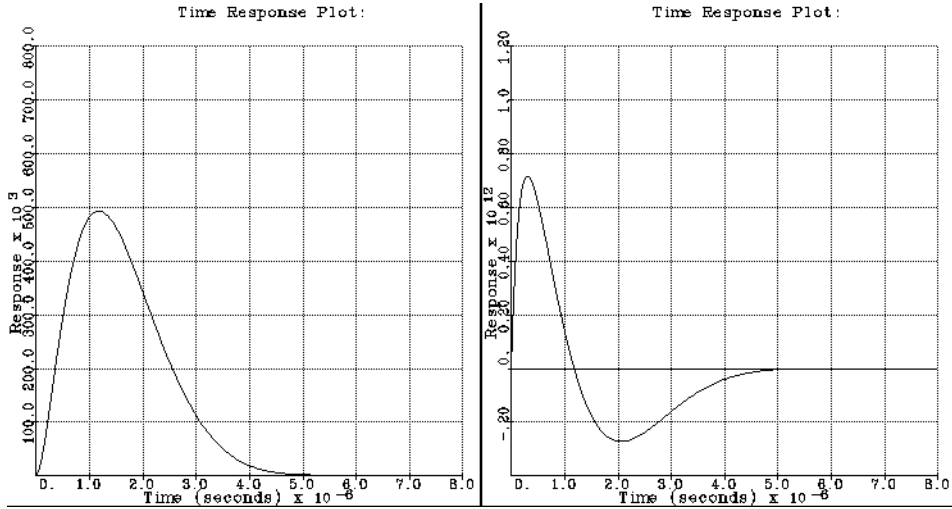
Figure 3-6: Pole at -1.05×10^6: **Critically Damped**
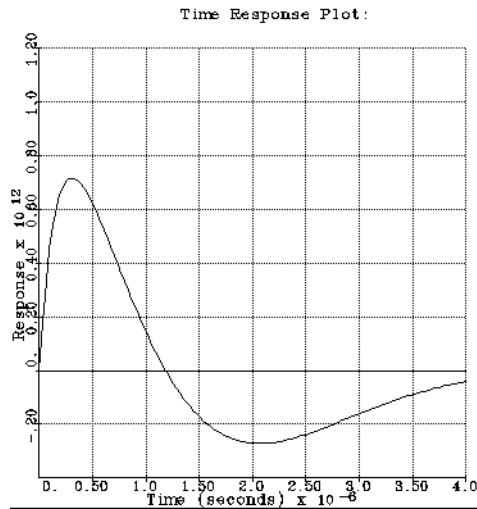
Figure 3-7: Zoomed Impulse Response with a Pole at -1.05×10^6

49
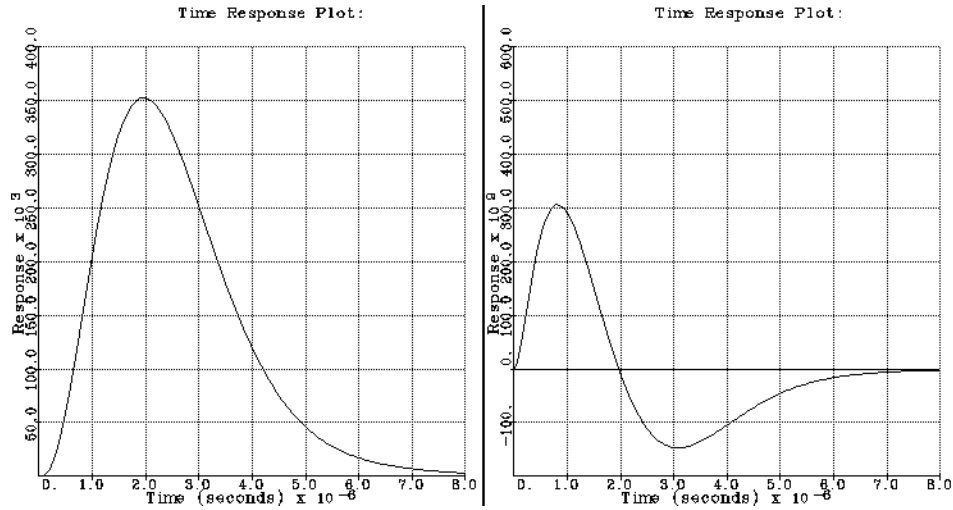
Figure 3-8: Two Poles at -1.05×10^6: Overdamped

model response, as discussed in section 1.3.3. Let us see then what kind of results can be obtained when another pole is added.

3.2   Second Pole

The additional degree of freedom makes the optimization problem more difficult than in the case of a single pole. At first let us start with the two poles on top of each other and move them together. Figures 3-8, 3-9, 3-10, and 3-11 show the step and impulse responses of such configurations, with the two poles positioned at interesting locations, such as the optimum one-pole position, and in between the complex pole pair. The first three configurations yield overdamped responses and the last one – an underdamped one.
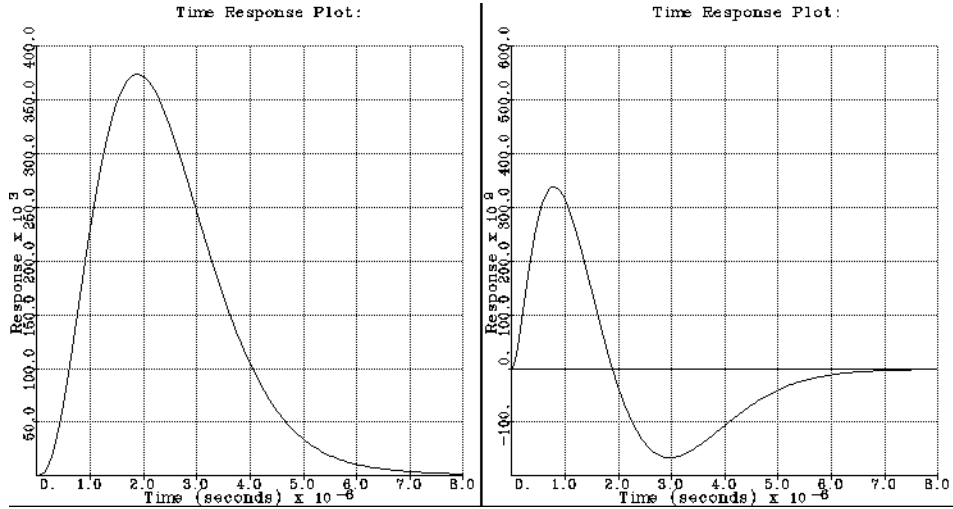
Figure 3-9: Two Poles at -1.14×10^6: Overdamped
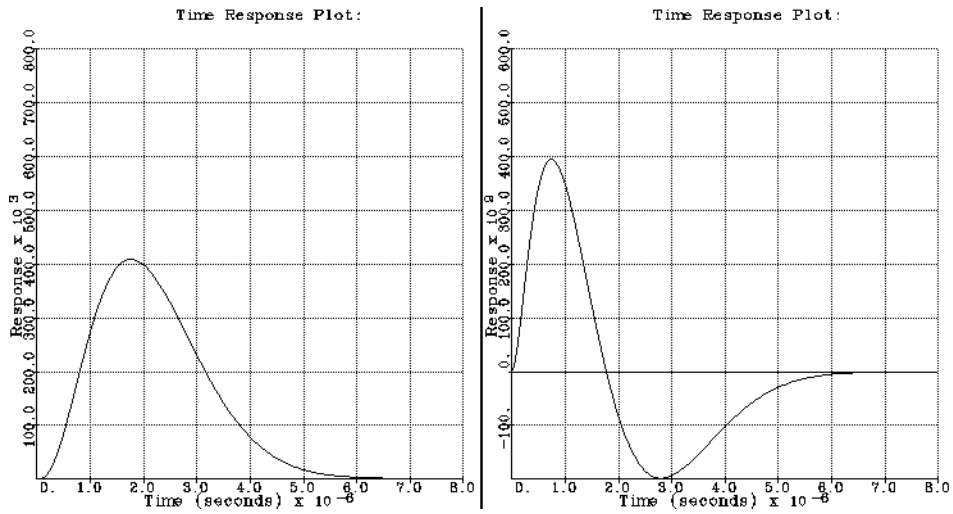
Figure 3-10: Two Poles at -1.30×10^6: Overdamped

51
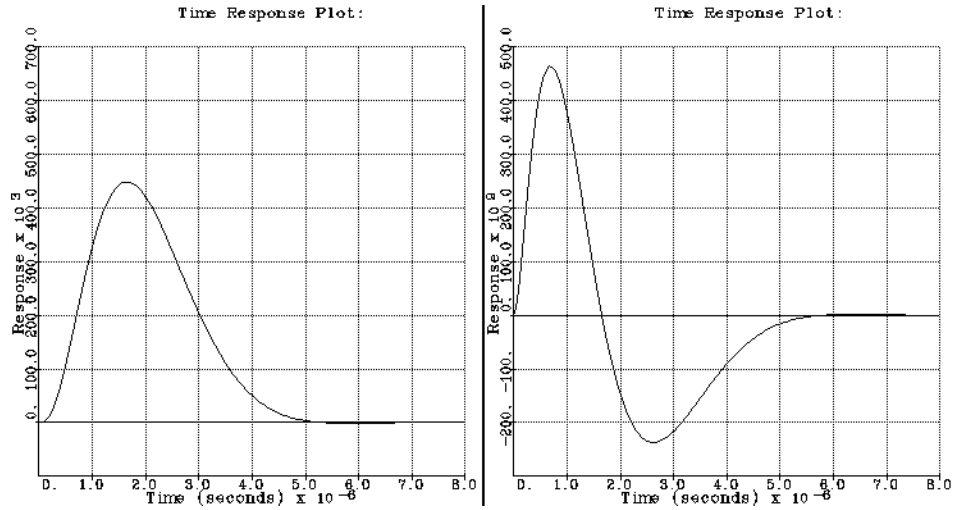
Figure 3-11: Two Poles at -1.50×10^6: Underdamped

Critical damping in the case of using two poles at the same location occurs at -1.40×10^6, as illustrated on figures 3-12 and 3-13. The efficiency is $E = 0.134$, which is much higher than that obtained by adding only a single pole. It is naturally so, since adding another pole makes a much better approximation to the true Gaussian.

There may be other configurations of two poles, of different values, which will yield a higher efficiency. Inspired by the pole-zero diagram of the Gaussian amplifiers, let us try keeping one of the poles at -1.14×10^6, between the two complex poles, and move the other one to reach critical damping. As seen on figures 3-14 and 3-15, critical damping occurs when the second pole is at -2.20×10^6, with efficiency of $E = 0.136$.

This is already an improvement. Following the same strategy, what happens if the pole at $3 \times (-1.14 \times 10^6) = -3.42 \times 10^6$ is steady and the other one is being moved until critical damping is achieved. The results are shown on figures 3-16 and 3-17. The efficiency in this case is down to $E = 0.117$.

In this last example the critical damping occurred when the second pole was moved to exactly the same value as when only a single pole was explored. (Figures 3-6 and 3-7) In the two-pole case, of course, the efficiency is much higher. Using this idea,

52
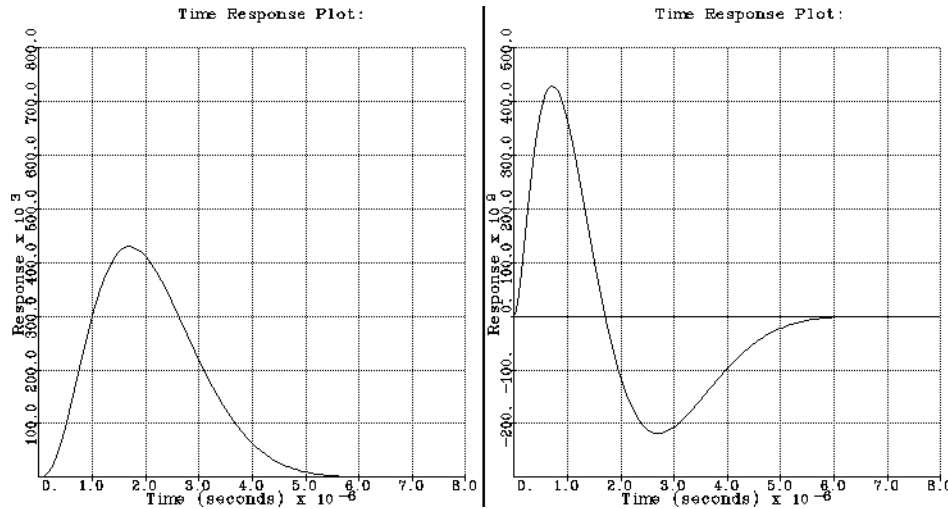
Figure 3-12: Two Poles at -1.40×10^6: **Critically Damped**
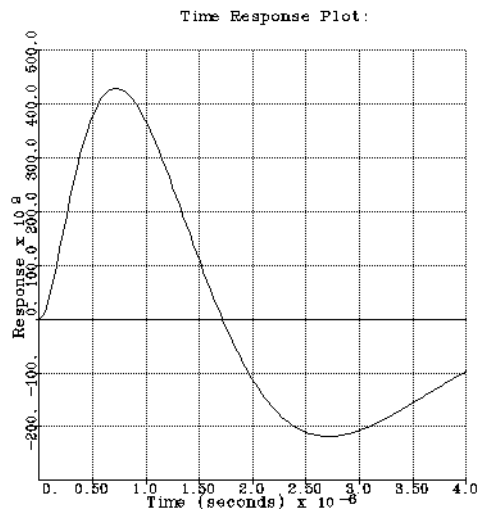
Figure 3-13: Zoomed Impulse Response with Poles at -1.40×10^6
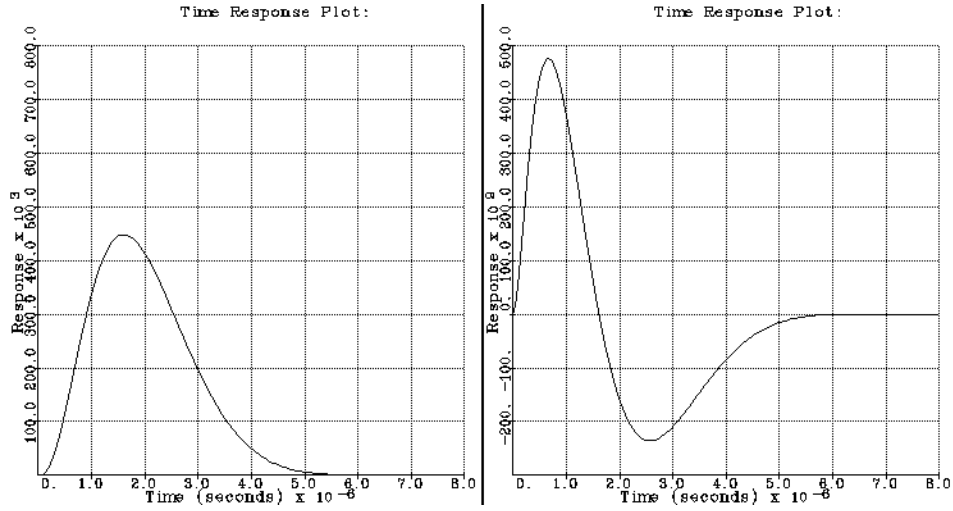
Figure 3-14: Poles at -1.14×10^6 and -2.20×10^6: **Critically Damped**
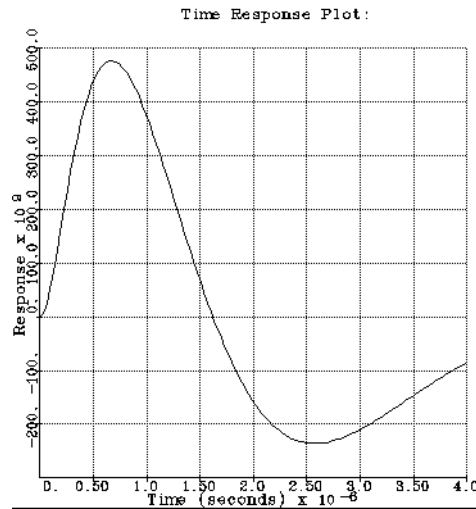
Figure 3-15: Zoomed Impulse Response with Poles at -1.40×10^6 and -2.20×10^6

54
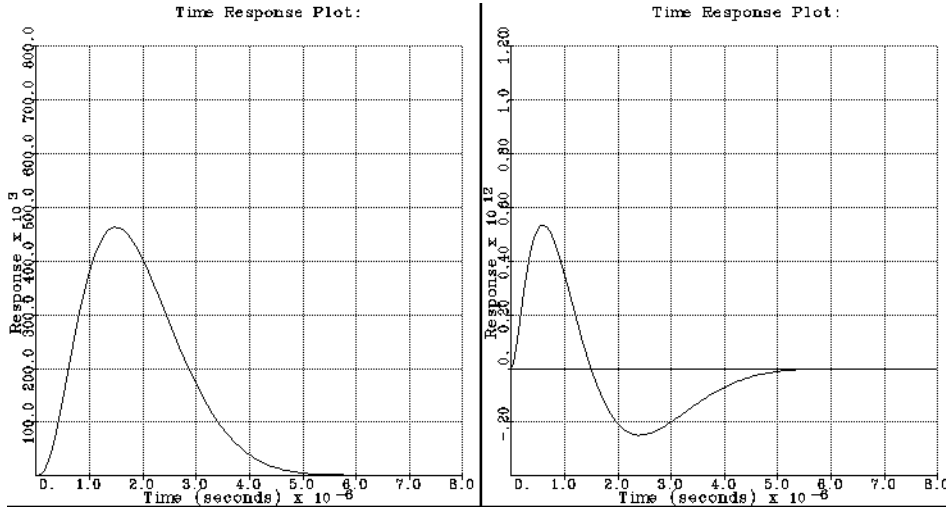
Figure 3-16: Poles at -1.05×10^6 and -3.42×10^6: **Critically Damped**
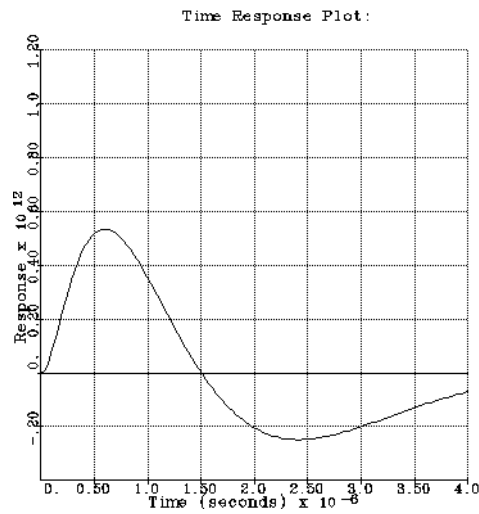
Figure 3-17: Zoomed Impulse Response with Poles at -1.05×10^6 and -3.42×10^6

55
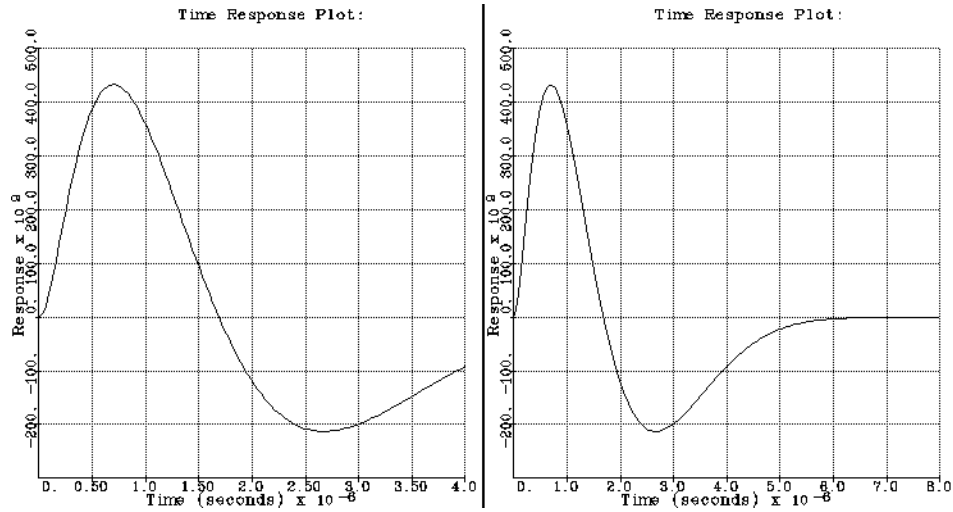
Figure 3-18: Impulse Response with Poles at -1.05×10^6 and -2.00×10^6

let's keep a pole at this very position, -1.05×10^6, and see what efficiency a critically damped system with this basic configuration would display.

Two such systems are shown on figures 3-18 and 3-19. These figures do not show the step response, but only the impulse response on two different time scales. The efficiencies are respectively $E = 0.130$ and $E = 0.125$.

The last few configurations are not as efficient as the one shown on figures 3-14 and 3-15, although the difference is not very significant.

All of the waveforms discussed in this chapter are summarized in table 3.1. The efficiency of each waveform is shown on figure 3-20. The table lists the number of the figure, the values of the additional poles, the damping, the corresponding efficiency, and the number on the bar chart shown on figure 3-20.

At this time it is reasonable to take the set of values on figures 3-14 and 3-15, -1.14×10^6 and -2.20×10^6, as the optimum solution, because it has the highest efficiency. The physical design of the amplifier stages should provide for some flexibility of fine tuning of the two poles. The pole-zero diagram of the overall system, as developed in this chapter, is shown on figure 3-21. It will be used in the physical implementation of the amplifier. Figure 3-22 once again shows the impulse response

56
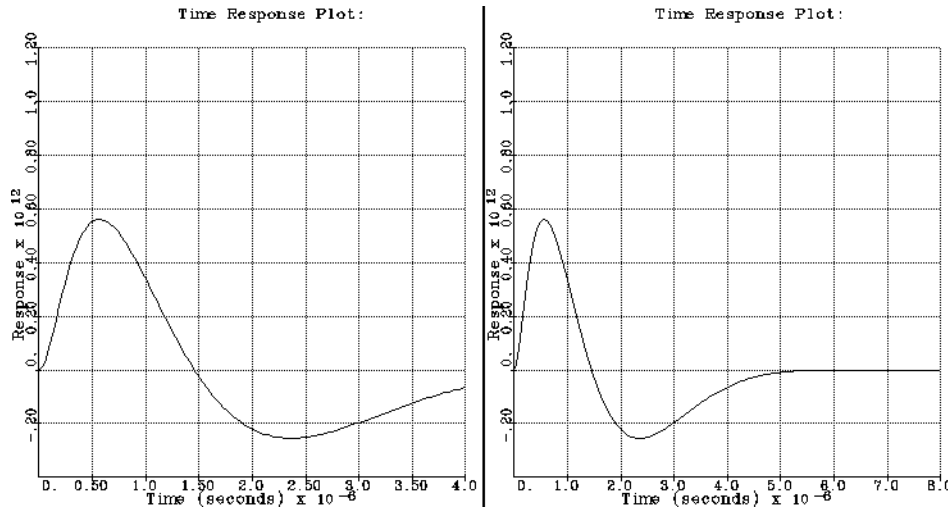
Figure 3-19: Impulse Response with Poles at -1.05×10^6 and -4.00×10^6

Figure	Poles	Damping	E	Bar #
3-1	-1.20×10^6	Under	0.0716	1
3-2	-1.14×10^6	Under	0.0795	2
3-3	-1.10×10^6	Under	0.0781	3
3-4	-0.90×10^6	Over	0.0903	4
3-5	-1.00×10^6	Over	0.0994	5
3-6	-1.05×10^6	Critical	0.108	6
3-8	-1.05×10^6 and -1.05×10^6	Over	0.106	7
3-9	-1.14×10^6 and -1.14×10^6	Over	0.108	8
3-10	-1.30×10^6 and -1.30×10^6	Over	0.119	9
3-11	-1.50×10^6 and -1.50×10^6	Under	0.101	10
3-12	-1.40×10^6 and -1.40×10^6	Critical	0.134	11
3-14	-1.14×10^6 and -2.20×10^6	Critical	0.136	12
3-16	-1.05×10^6 and -3.42×10^6	Critical	0.117	13
3-18	-1.05×10^6 and -2.00×10^6	Critical	0.130	14
3-19	-1.05×10^6 and -4.00×10^6	Critical	0.125	15

Table 3.1: Summary of the Waveforms in Chapter 3
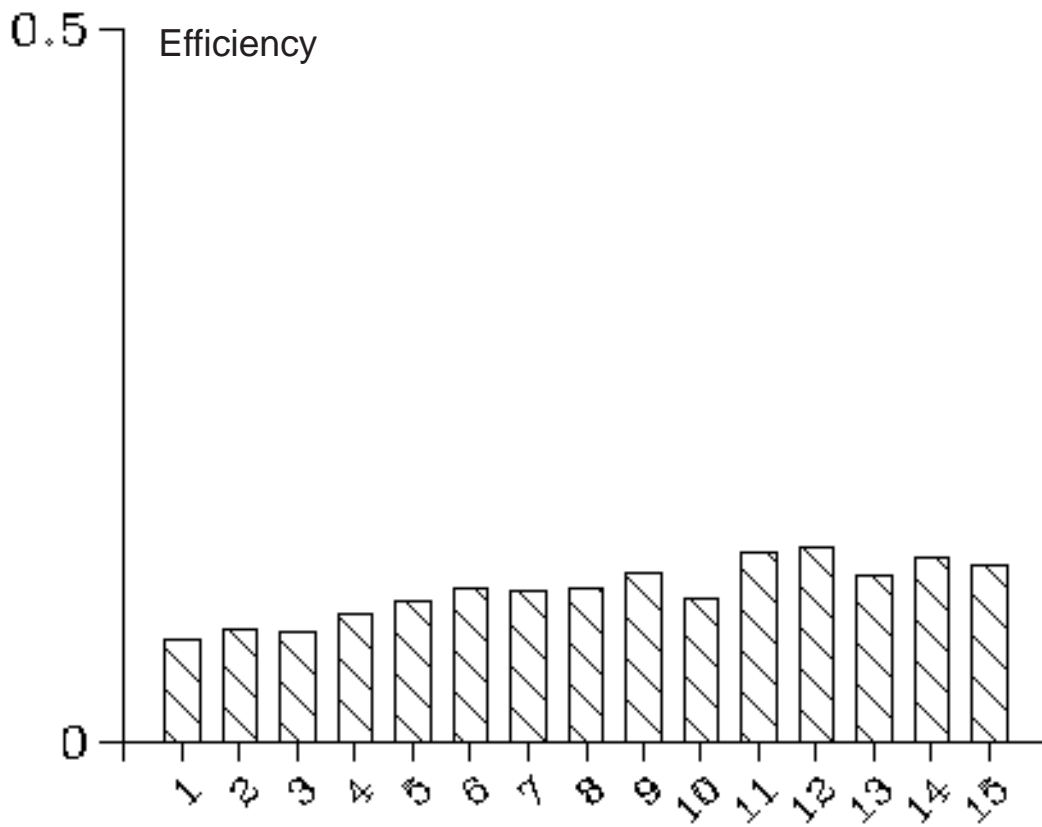
Figure 3-20: Summary of the Efficiency of the Waveforms in Chapter 3
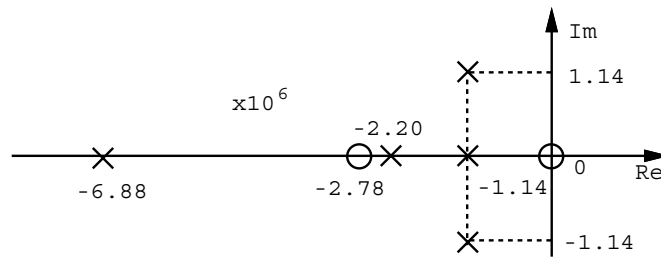
Figure 3-21: Pole-Zero Diagram of the Overall System, i.e. Sensor and Filter

of this optimal system, and it also shows its frequency behaviour.

The possibility exists, of course, of adding more poles. With each additional pole the system's response will be closer to the gaussian derivative, in keeping with the trend outlined in section 1.3.1. (A true gaussian requires an infinite number of poles.) However, the cost of adding more filter stages does not justify the minor improvement in the signal-vs-noise characteristics. This is why I chose to follow the design strategy of the ORTEC gaussian amplifiers in the first place, represented by their pole-zero configurations.

Time Response Plot:

Bode Magnitude and Phase Response in s:
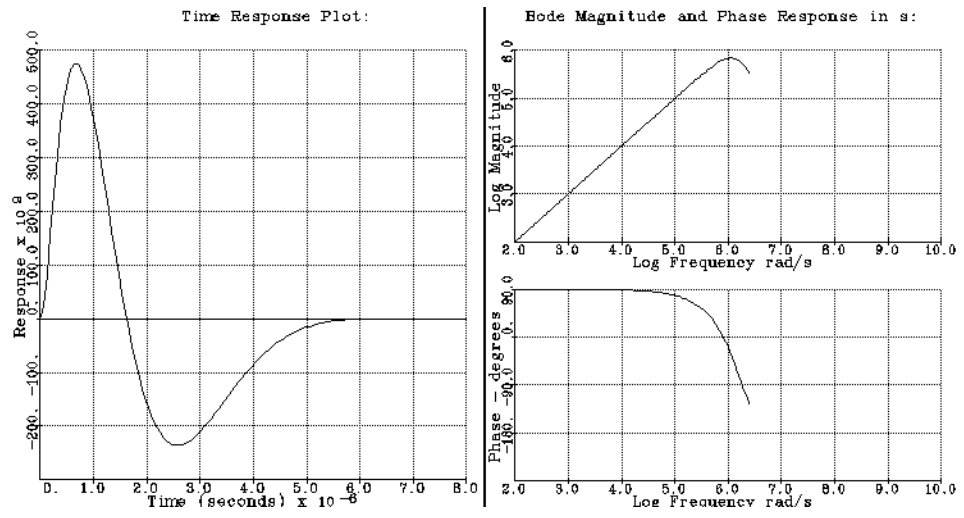
Figure 3-22: Impulse Response and Bode Plot of the Overall System

60

Chapter 4

Physical Implementation and Measurements

In this chapter I consider the physical implementation of the system developed in the previous two chapters. Its pole-zero diagram can be seen on figure 3-21. The overall system consists of the following stages:

- Current Sensor. For reasons outlined in chapter 2 I have chosen sensor type PPD-102X. It is loaded with a $4.7nF$ capacitor and the input impedance of the preamplifier.

- Preamplifier. This stage is used to provide gain at the front end. In this way the thermal noise of the subsequent filter stages will not significantly affect the signal-to-noise ratio. I have considered using low-noise preamplifiers models W500C or W40F. This choice is considered in more detail in section 4.2.

- Filter. This is a two-stage filter, adding the two poles discussed in the previous chapter. Each of the two stages may be tuned independently. The output of the second stage is the output of the whole system.

The circuit diagram of the system, together with a set of possible component values, is shown on figure 4-1. It is important to calculate the sensitivity of this system, represented by the previously defined quantity MDS (Q_C).
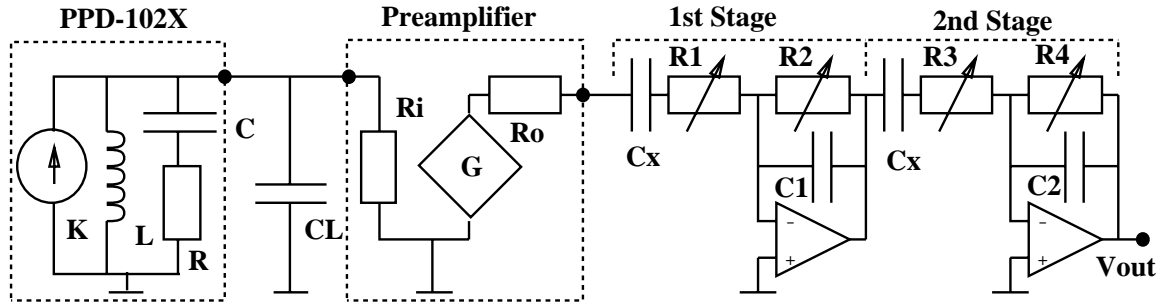
$$K = 1/3 = 0.33 \qquad C_L = 4.7nF \qquad C_X = 0.1\mu F \text{ (coupling)}$$
$$L = 33\mu H \qquad R_L = R_i = 50\Omega$$
$$C = 3.6nF \qquad G = 42dB$$
$$R = 100\Omega$$

Figure 4-1: Overall System Circuit Diagram

4.1 *Sensitivity*

In order to calculate the MDS of this system, we need two quantities: the RMS value of the thermal noise voltage at the output, and the peak voltage at the output per unit charge of current pulse area. In order to simplify the calculations, all gains of the system are ignored, as they do not affect the signal-to-noise ratio.

The output-to-noise system function is obtained when the two new poles are added to equation 2.3. The values obtained for the two poles in the previous chapter are:

$$p_1 = 0.114 \times 10^7 \qquad\qquad p_2 = 0.220 \times 10^7$$

Therefore the overall noise system function is:

$$\frac{V_{out}}{V_N} = \frac{1}{RC_L} \cdot \frac{s^2}{[s^3 + (\frac{1}{RC_L} + \frac{1}{RC} + \frac{1}{R_L C_L})s^2 + (\frac{1}{LC_L} + \frac{1}{RR_L CC_L})s + \frac{1}{LRCC_L}](s + p_1)(s + p_2)}$$
$$(4.1)$$

To find the peak value in frequency of this transfer function, a numerical calculation of bode data is carried on, and then the results are read directly from the graph.
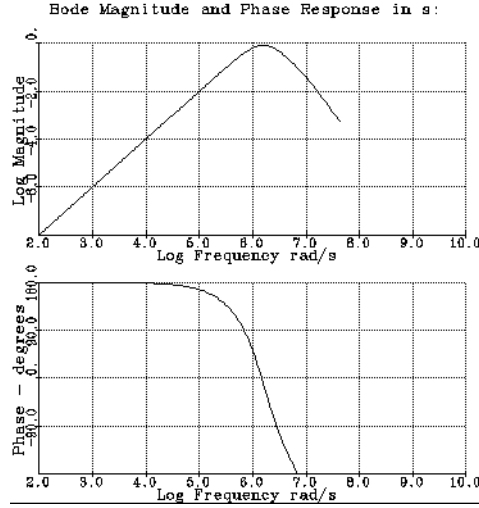
Figure 4-2: Calculated Noise Transfer Function Bode Plots

The bode plot of this transfer function is shown on figure 4-2. Figure 4-3 shows the peak of the magnitude plot in more detail on a different scale. When the pole-zero configuration was entered into the program in order to calculate the data on these figures, the Bode gain was set to 10^{-12}, for a clearer plot. In order to be able to read useful data from the plot, we must first convert equation 4.1 to standard Bode form. Here is the result:

$$\frac{V_{out}}{V_N} = \frac{LC}{p_1 p_2} \cdot 10^{12} \frac{10^{-12} s^2}{[1 + (RC + \frac{L}{R_L})s + (\frac{RLC}{R_L} + LC + LC_L)s^2 + LRCC_L s^3](1 + \frac{s}{p_1})(1 + \frac{s}{p_2})}$$
$$(4.2)$$

The braces enclose the system function entered for the numerical calculation of the data on the Bode plots.

Since thermal noise generation depends on the bandwidth, I consider the bandwidth to be limited by the frequency at which the magnitude has dropped $3dB$ below its peak value. On figure 4-3 the peak is at point A, where the magnitude is $10^{-0.0755}$. $3dB$ down form point A is point B, where the magnitude is down to $10^{-0.0755 - \frac{3}{20}} = 10^{-0.226}$. Point B occurs at frequency $\frac{10^{6.413}}{2\pi} = 412kHz$. Therefore the

63
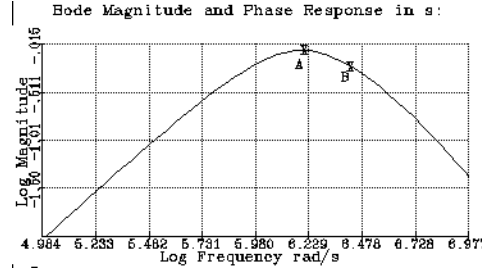
Figure 4-3: Calculated Enlarged Magnitude Bode Plot

value for the bandwidth is $\Delta f = 412kHz$. The value of the magnitude at point B, which should be substituted for the expression in braces in equation 4.2, is $10^{-0.226}$. At this point we are ready to calculate the maximum value of $\frac{V_{out}}{V_N}$:

$$\frac{V_{out}}{V_N}(max) = \frac{LC}{p_1 p_2} \cdot 10^{12} \cdot 10^{-0.226} = 2.82 \times 10^{-14} \tag{4.3}$$

The RMS value of the voltage at the output is, therefore:

$$V_{ON} = \sqrt{4RkT\Delta f} \times \frac{V_{out}}{V_N}(max) = 2.32 \times 10^{-20}V \tag{4.4}$$

The value so obtained is meaningful only in the calculation of the MDS, because all gains were ignored.

Now we need to find $V_{out}(max)$ per unit charge. The maximum value will be read from the plot shown on figure 3-15. Since the data for the plot was entered in standard Bode format, a conversion factor will be used, as in the procedures used above. The maximum value on the plot is 477×10^9. Using equation 2.2, we get:

$$\frac{V_{out}}{Q}(max) = \frac{K}{C_L} \cdot \frac{LRCC_L}{RCp_1 p_2} \cdot 477 \times 10^9 = 2.08 \times 10^{-6}V/C \tag{4.5}$$

The MDS can now be obtained by dividing equation 4.4 by equation 4.5:

$$Q_C = \frac{2.32 \times 10^{-20}}{2.08 \times 10^{-6}} = 11.2 fC \qquad (4.6)$$

As discussed earlier, the minimum detectable current pulse area, which would yield useful information, would have to be a few times larger than the so calculated MDS.

4.2   *Preamplifier*

The preamplifier is the stage following the capacitively loaded current sensor. Its input impedance serves as the load resistance of the current sensor. The preamplifier's function is to make any thermal noise generated in the stages following it insignificant compared to the noise generated in the current sensor. Therefore the most important requirement is that the preamplifier be as low-noise as possible and with significant gain in the frequency band of interest.

The two preamplifiers available to me are models W40F and W500C. Both of them have input and output impedance of 50Ω. They have gains of $46dB$ and $42dB$ respectively. The major difference between them lies in their frequency response. I shall consider each one separately.

4.2.1   Model W40F

This is a broad-band amplifier, with an estimated bandwidth of $300kHz$ to $40MHz$. While its high-frequency range of operation is not useful in this application, its low-frequency roll-off may present a problem. Its step response is shown on figure 4-4 [1]. It's driven by a 50Ω signal generator and its output is also terminated at 50Ω.

This behaviour can be accurately described by a zero at the origin and a pole with a time constant of $0.5\mu s$. This configuration and its predicted step response may be seen on figure 4-5. The predicted response matches the experimental one quite well, thus confirming this simple model. The zero at the origin has an important advantage:

---

[1]The equipment used to take this and subsequent photographs is discussed in the appendix
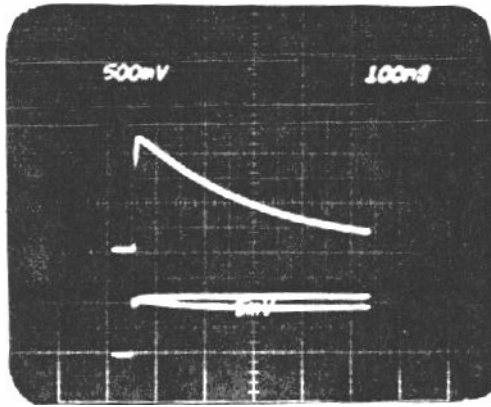
Trace	Description	Units
Top	Output into 50Ω	$500mV/smdiv$
Middle	Drive into 50Ω	$5mV/smdiv$
Bottom	Drive into amp.	$5mV/smdiv$
Sweep		$100ns/smdiv$

Figure 4-4: W40F Step Response
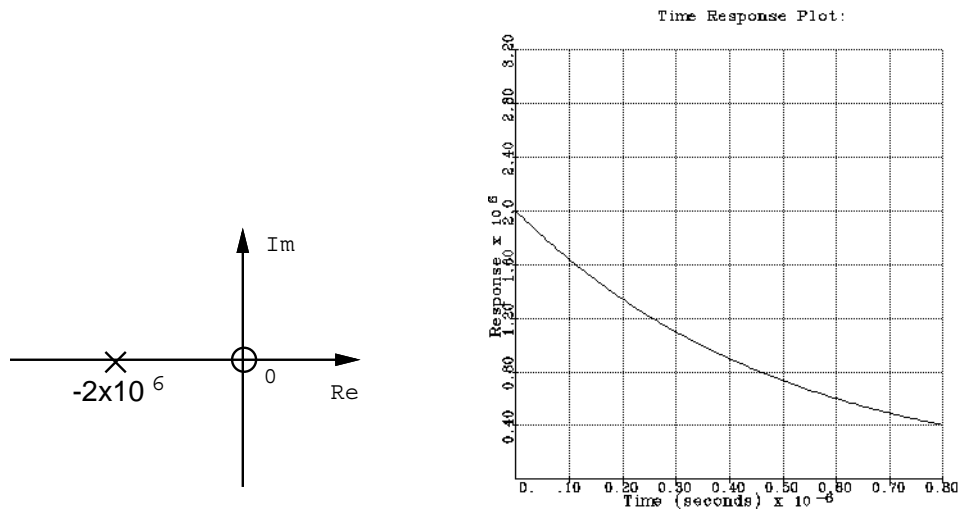
Figure 4-5: PZ Model and Predicted Step Response of W40F

the low-frequency roll-off is twice faster and therefore the amount of low-frequency noise, generated by the ambient $60Hz$ background, is greatly attenuated. On the other hand, it is in effect a differentiation and will change the shape of the waveform at the output.

Since the extra pole and zero, introduced by the non-ideal preamplifier, change the overall system function, the set of two extra poles, developed in the previous chapter, do not yield the optimum configuration. Therefore I will try to see what other filtering may work better if this preamplifier is used.

Figure 4-6 shows the step and the impulse responses of a system including the
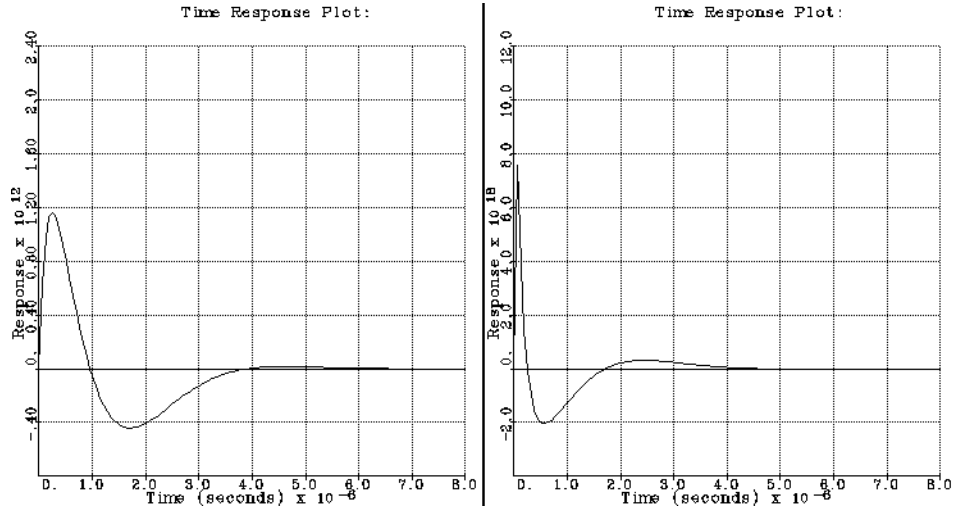
Figure 4-6: Calculated Step and Impulse Response of Current Sensor and W40F Preamplifier. No Filtering

current sensor, capacitively loaded, and the preamplifier W40F. The response is approximately the derivative of what it should be, i.e. of that shown on figure 3-14, which is due to the zero at the origin. As a first try we may try to cancel this zero by adding a very slow pole. (A pole at the origin would be ideal, but it is not possible to implement.) The result is shown on figure 4-7. The impulse response is close to what we want, but the step response shows a slow tail. This is very undesirable, because it causes progressively accumulating errors.

If we now try to add a faster pole instead, comparable with the other poles of the system, we get the results shown on figure 4-8. The problem with this waveform is that the peak of the impulse response occurs too early and the positive area is split in two parts, of which only the first one is of importance. Therefore the peak represents only a fraction of the energy of the pulse.

An attempt to slow the arrival of the peak, as compared to the total duration of the waveform, is made by adding another pole (figure 4-9). Now the impulse response starts at a lower slope and its peak arrives later.

A more efficient solution with the same idea is shown on figure 4-10, where by
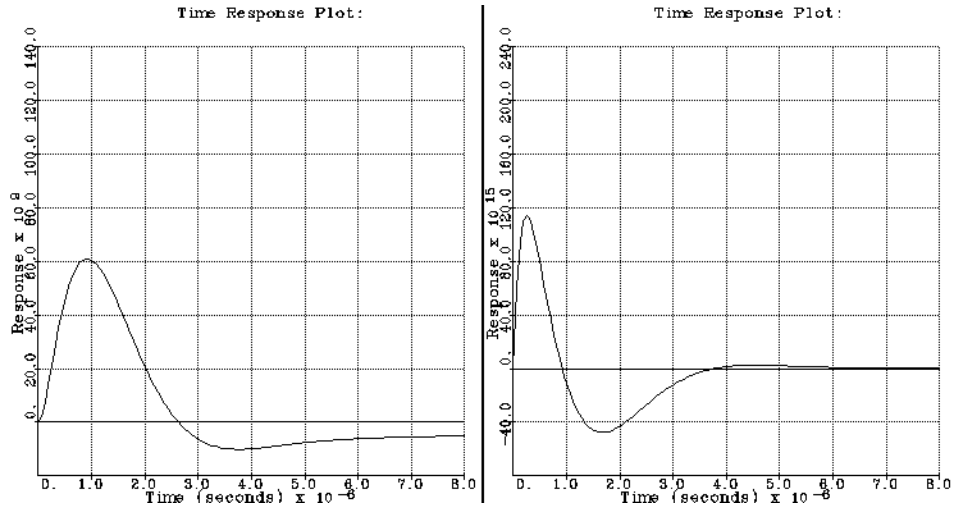
Figure 4-7: Responses with W40F and One Pole at -1×10^5
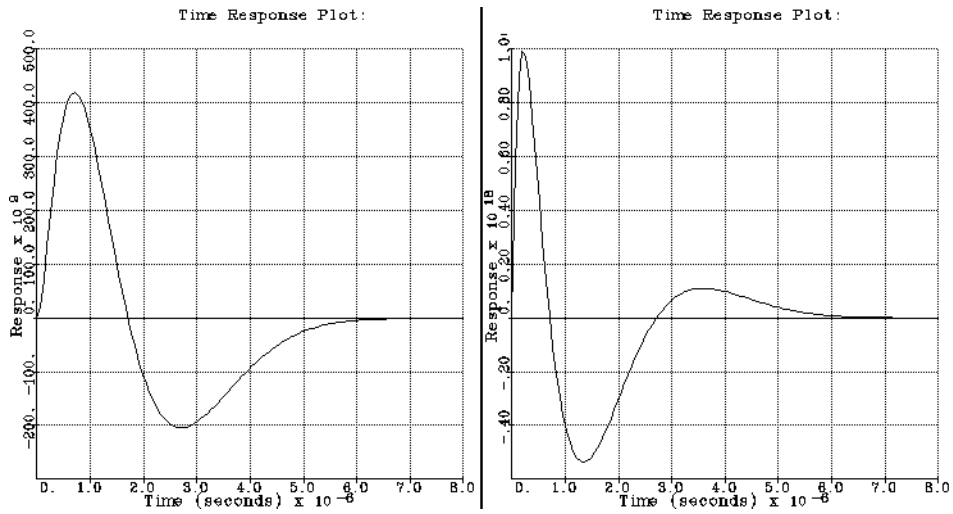
Figure 4-8: Responses with W40F and One Pole at -1×10^6
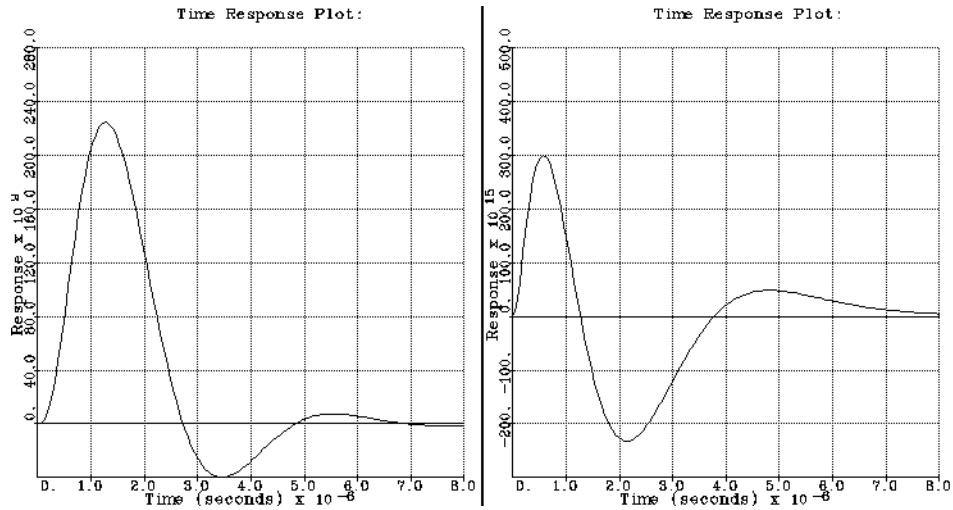
Figure 4-9: Responses with W40F and Two Poles at -1×10^6

moving the poles critical damping is achieved. This is the best response that could be achieved with W40F. The efficiency is really low, $(E = 0.0734)$, but this is not the only problem. As noted earlier, the peak value per unit input charge is low because a smaller fraction of the energy has gone into the first peak.

This is why a better design would make use of the other preamplifier, W500C, since the poles and zeros that it introduces may be compensated for in a later stage.

4.2.2   Model W500C

This amplifier's frequency range is not as high as that of W40F. Its experimentally measured step response, taken under the same conditions as the step response of W40F, are shown on figures 4-11 and 4-12. The two pictures are taken at different sweep rates.

The step response makes a step, whose rise time is comparable to that of the signal generator and therefore negligible, and then proceeds to rise to its final value, following an exponential. This behaviour occurs when a pole-zero pair is present, with the pole having the longer time constant. (See equivalent circuit on figure 4-24.
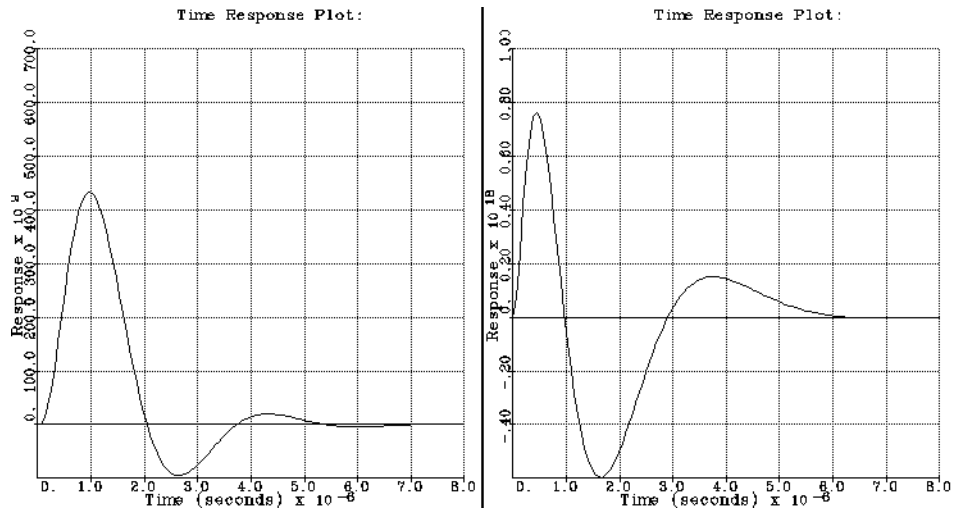
Figure 4-10: Responses with W40F and Two Poles at -2×10^6
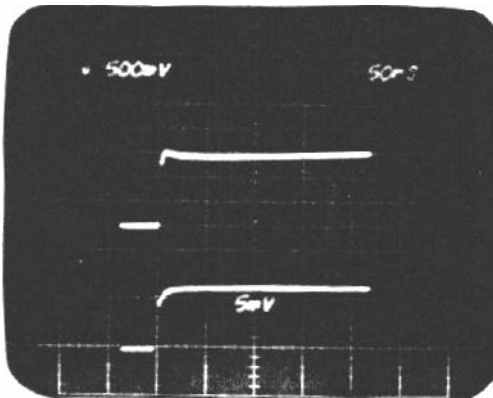
Trace	Description	Units
Top	Output into 50Ω	$500mV/smdiv$
Bottom	Drive into amp.	$5mV/smdiv$
Sweep		$50ns/smdiv$

Figure 4-11: W500C Step Response (Fast Sweep)
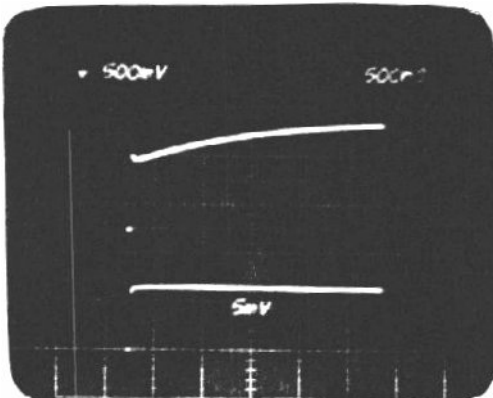
Trace	Description	Units
Top	Output into 50Ω	$500mV/smdiv$
Bottom	Drive into amp.	$5mV/smdiv$
Sweep		$500ns/smdiv$

Figure 4-12: W500C Step Response (Slow Sweep)

70
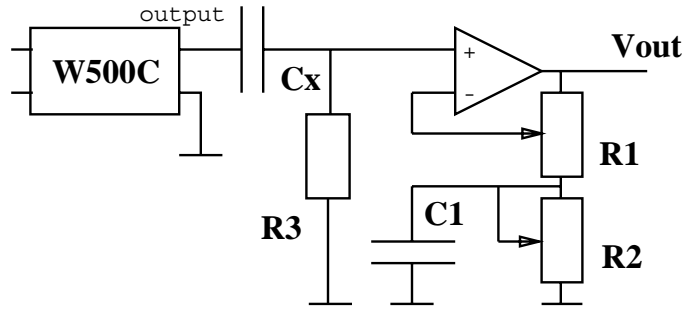
$$C_x = 0.1\mu F \quad \text{op. amp. LF356} \quad R_1 = 5k\Omega \text{ (pot.)}$$
$$R_3 = 5.6k\Omega \qquad\qquad\qquad R_2 = 5k\Omega \text{ (pot.)}$$
$$C = 2.0nF$$

Figure 4-13: Compensation Stage Circuit Diagram

Neither of these are at the origin and may be compensated at a later stage. This is the strategy I chose to use. The compensation stage for the W500C amplifier is developed in the next section.

4.2.3   Compensation for W500C

The compensation stage must have a quick pole and a slow zero, each tuned independently. This can be achieved by an amplifier, whose initial gain factor exponentially decreases to a new value. The schematic diagram of one such configuration is shown on figure 4-13. α and β stand for the position of the potentiometer gliders of R_1 and R_2 respectively and take values from 0 to 1. If we assume the operational amplifier is ideal, the transfer function of this stage would be:

$$\frac{V_{out}}{V_{in}} = \frac{\alpha R_1 + \beta R_2}{R_1 + \beta R_2} \cdot \frac{1 + (\alpha R_1 \parallel \beta R_2)C_1 s}{1 + (R_1 \parallel \beta R_2)C_1 s} \qquad (4.7)$$

The two degrees of freedom, α and β, let us position the pole and the zero so that they match and cancel those of the W500C amplifier. The position of the pole depends only on β, so it should be set first. I physically implemented this stage, using the component values listed on the figure. The measured step response of this
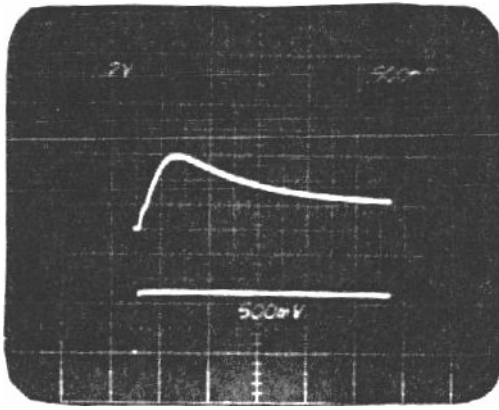
Trace	Description	Units
Top	Output (unloaded)	$2V/smdiv$
Bottom	Drive into stage	$500mV/smdiv$
Sweep		$500ns/smdiv$

Figure 4-14: Compensation Stage Step Response
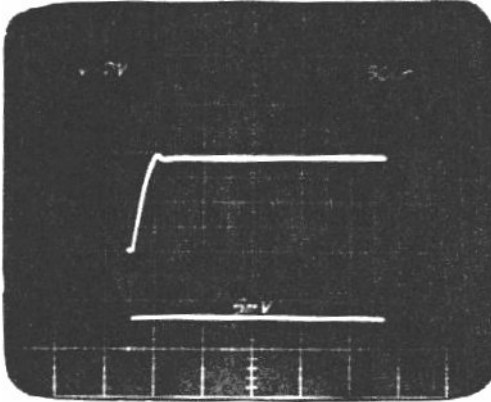
Trace	Description	Units
Top	Output (unloaded)	$2V/smdiv$
Bottom	Drive into W500C	$5mV/smdiv$
Sweep		$500ns/smdiv$

Figure 4-15: Compensated W500C Step Response

compensation stage is shown on figure 4-14. It manifests the expected behaviour, with one notable exception: its finite rise time. This is due to the presence of another pole, introduced by the non-ideal operational amplifier. Although LF356 is a fast amplifier, it is frequency compensated and does introduce another pole. The effect of this extra pole will be discussed later.

The tuning of the compensation stage involves watching the step response of the two stages, the preamplifier and the compensation stage, and adjusting the values of the potentiometers so that the output is as close to a step as possible. After tuning, the experimental step response of the compensated W500C is shown on figure 4-15. This behaviour is that of a single-pole first-order system, whose time constant is determined by the rise time of the step.

Now let us look at the overall system created so far. At this point I would like to test what the output of the compensation stage would yield when excited by a step of current through the current sensor. The experimental setup used to take these measurements is shown on figure 4-16. The signal generator creates a step of voltage.

72
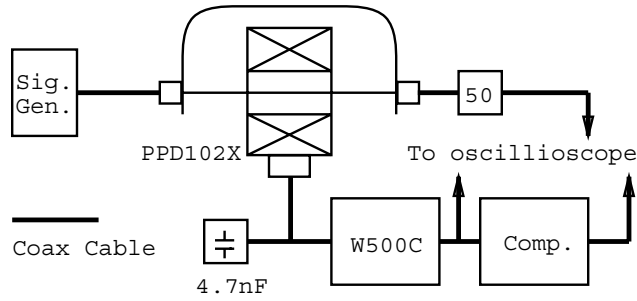
Figure 4-16: Experimental Setup for Figures 4-17, 4-19 and 4-21
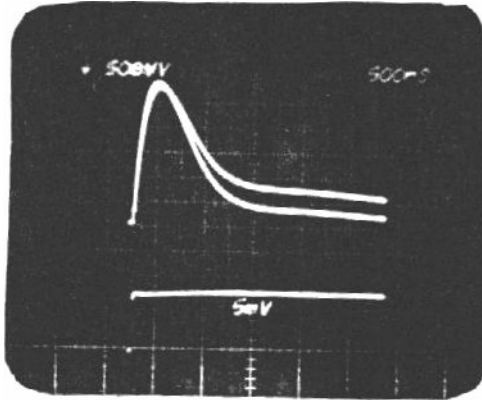
Trace	Description	Units
Top	Output (unloaded)	$1V/smdiv$
Middle	Output into 50Ω	$500mV/smdiv$
Bottom	Drive through sensor into 50Ω	$5mV/smdiv$
Sweep		$500ns/smdiv$

Figure 4-17: PPD-102X and Non-Compensated W500C Step Response

After passing through the coil of the current sensor, this signal terminates into 50Ω at one of the inputs of the oscilloscope (a matched load). The current through the coil is therefore directly proportional to the voltage registered by the oscilloscope, with a proportionality constant of $(50\Omega)^{-1}$.

Figure 4-17 shows what the step response of the system is if no compensation is used, i.e. only the capacitively loaded PPD-102X and W500C. Both the unloaded and the 50Ω-load cases are shown. Both traces manifest a slowly decaying tail, as expected. The tail decays at the rate determined by the pole of the W500C amplifier.

After the compensation stage is added, however, the long tail is gone. The experimental step and impulse responses of this system now are shown on figure 4-19. The step response shown on this figure is measured using the setup shown on figure 4-16. The impulse response, however, requires a change in the drive circuitry. The line
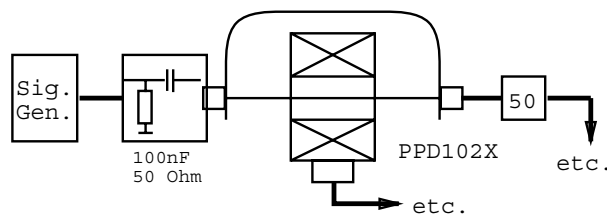
Figure 4-18: Modified Experimental Setup Used to Measure Impulse Response

coming from the pulse generator is terminated into 50Ω prior to the current sensor. A series $100pF$-capacitor shapes the pulse through the sensor, which is then terminated into 50Ω at the oscilloscope. Figure 4-18 shows this setup modification.

In order to compare how this system's response differs from the numerically calculated one, the latter is shown on figure 4-20. It does not include the pole introduced by the slow operational amplifier. Therefore the compensated W500C is assumed to be pure gain and the only poles and zeros are those introduced by the loaded current sensor.

There are two major differences between the predicted and the experimental responses:

- At $t = 0$, the measured step response starts up with zero slope, unlike the predicted response, which starts up with a finite positive slope. Analogously, the measured impulse response has a finite rise time, whereas on the predicted impulse response the rise time is zero. Both of these phenomena are due to the extra fast pole, due to the slow operational amplifier in the compensation stage. The numerical calculation does not take it into account.

- Theoretically the impulse response should terminate after it goes below zero. The experimental response, however, shows one more oscillation of low, but visible, magnitude. A similar oscillation may be seen in the step response. In order to find where in the system this problem arises, I compare the responses shown on figure 4-19 to those on figure 4-21. The latter are taken when the
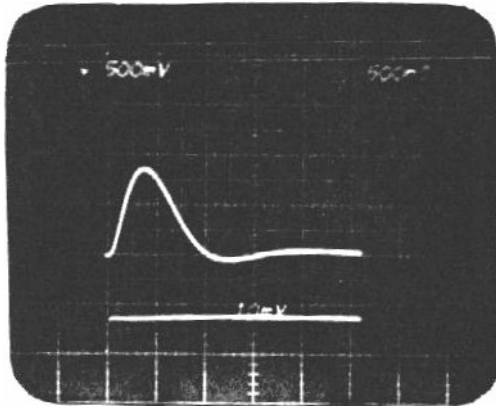
74

Trace	Description	Units
Top	Output (unloaded)	$500mV$ /$smdiv$
Bottom	Drive through sensor into scope	$10mV$ /$smdiv$
Sweep		$500ns$ /$smdiv$
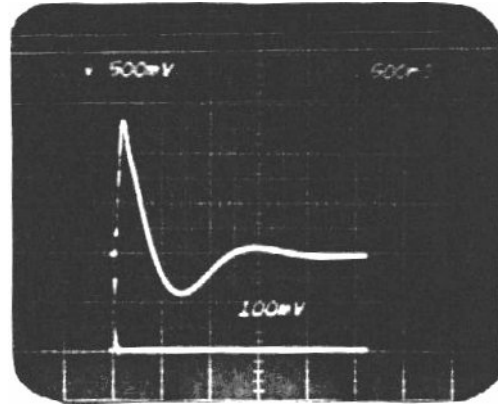
Trace	Description	Units
Top	Output (unloaded)	$500mV$ /$smdiv$
Bottom	Drive through sensor (series cap.)	$100mV$ /$smdiv$
Sweep		$500ns$ /$smdiv$

Figure 4-19: Step and Impulse Response of PPD-102X and Compensated W500C

current sensor is loaded with the $4.7nF$-capacitor and a discrete 50Ω-resistor, with no amplifiers. These agree perfectly with the predicted responses, shown on figure 4-20. This means that the reason the responses ring when the amplifier stages are added is that the input impedance of the W500C preamplifier does not look like 50Ω at all times. It has some reactance, which interferes with the system function of the loaded current sensor.

The first problem is not very significant, since the extra pole is of a lower time constant than the other poles in the system and may in fact be used in the filtering stage to help shape the waveform for maximum efficiency. The second problem may probably be fixed by finding a new optimum value for the loading capacitor at the front end.
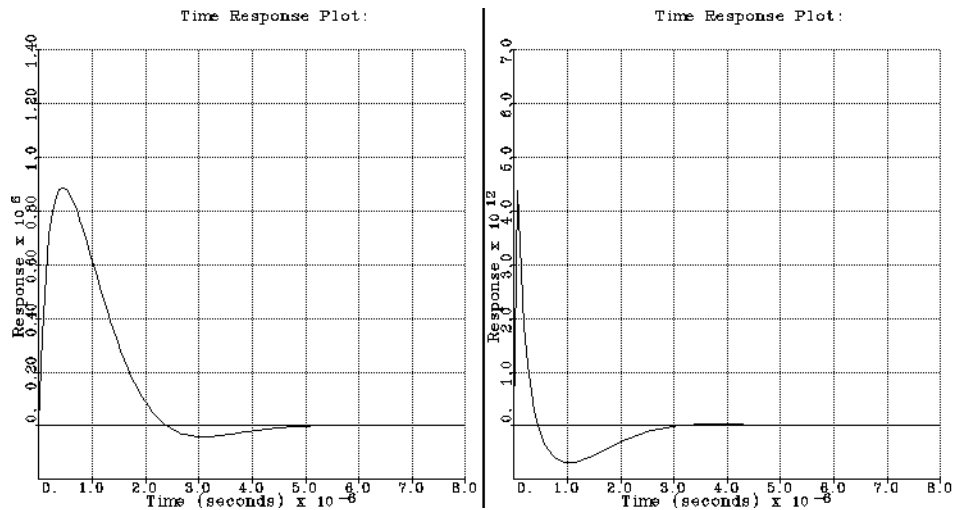
Figure 4-20: Predicted Step and Impulse Response of Loaded PPD-102X
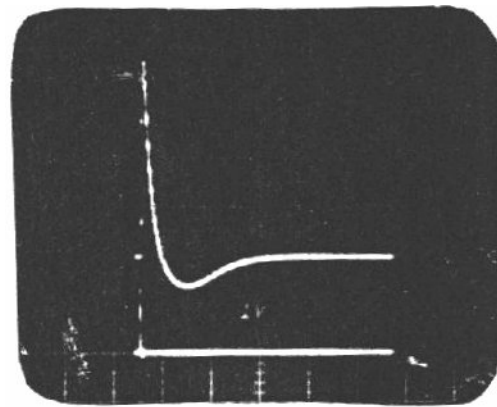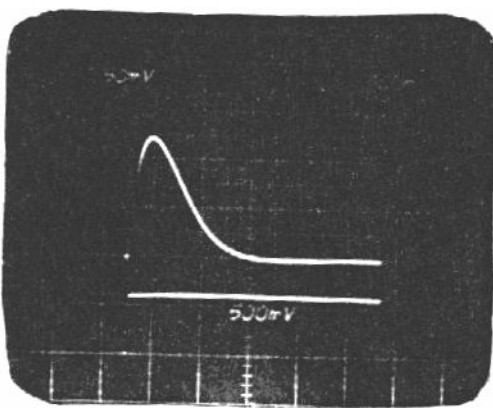
Trace	Description	Units
Top	Output into 50Ω	$50mV$ $/smdiv$
Bottom	Drive through sensor into scope	$500mV$ $/smdiv$
Sweep		$500ns$ $/smdiv$

Trace	Description	Units
Top	Output into 50Ω	$5mV$ $/smdiv$
Bottom	Drive through sensor (series cap.)	$1V$ $/smdiv$
Sweep		$500ns$ $/smdiv$

Figure 4-21: Step and Impulse Response of PPD-102X Loaded with 50Ω

4.3   Final Design

In the previous section I discussed the effect of the extra pole, which the frequency compensated operational amplifier of the compensation stage adds to the overall system transfer function. Because of its presence I choose to add only one more stage to the filter, in order to make the physical design simpler.

The circuit diagram of this last stage is shown on figure 4-22. This configuration adds a single pole, whose position may be altered by the value of R_5. R_4 is a gain control. This stage, of course, is also used to provide gain. The operational amplifier is the same as in the previous stage and it will add another fast pole. Assuming an ideal operational amplifier, the transfer function of this stage is:

$$\frac{V_{out}}{V_{in}} = -\frac{R_5}{R_4(1 + R_5 C_2 S)} \tag{4.8}$$

Figure 4-23 shows the experimental step and impulse response of the overall system. Its total circuit diagram is shown on figure 4-24. The W500C amplifier and the compensation stage together implement a gain stage. Therefore this particular design is specific to the use of this preamplifier. Figure 4-25 shows the structure of the system built in its more generic form. There the combination of these two stages is represented with a single gain stage introducing only one pole due to the operational amplifier of the compensation stage.

4.4   Test of Sensitivity

The final experimental test of the physically implemented system is a test of its sensitivity. Its response to a pulse of current is shown on figure 4-23. The question is how small this pulse of current can be, with the output waveform still distinguishable against the background of thermal noise.

The experimental setup is shown on figure 4-26. The signal generator has built-in attenuation. The signal is further attenuated by a series of 50Ω coaxial cable attenuators ($20dB + 6dB = 26dB$, i.e. $\frac{1}{40}$) and then terminated at 50Ω. The oscilloscope is
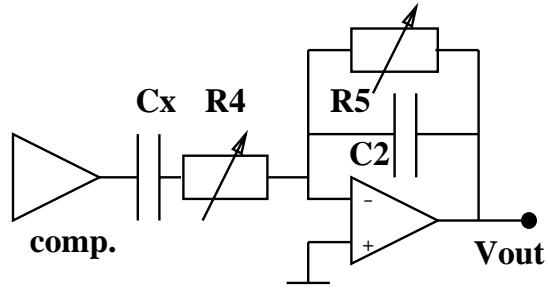
$C_x = 0.1\mu F \qquad C_2 = 200pF \qquad R_4 = 1k\Omega$ (pot.)
(coupling) op. amp. LF356 $\quad R_5 = 5k\Omega$ (pot.)

Figure 4-22: Circuit Diagram of the Last Filter Stage
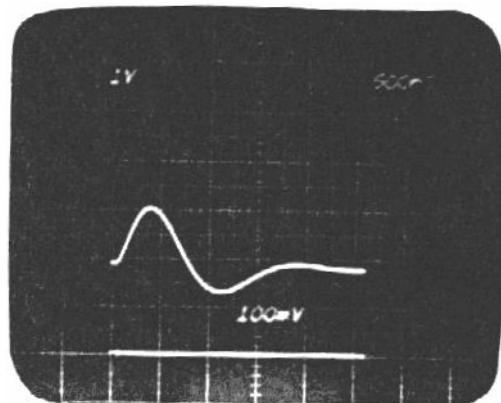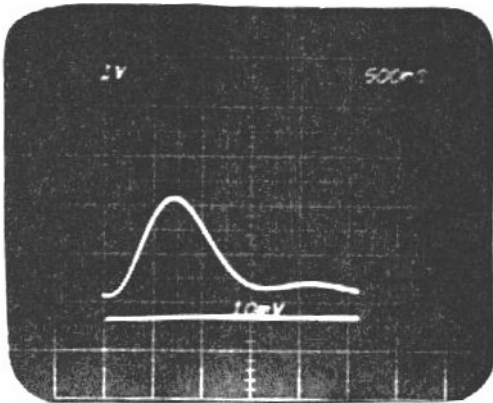
Trace	Description	Units
Top	Output	$1V$ $/smdiv$
Bottom	Drive through sensor into scope	$10mV$ $/smdiv$
Sweep		$500ns$ $/smdiv$

Trace	Description	Units
Top	Output	$1V$ $/smdiv$
Bottom	Drive through sensor (series cap.)	$100mV$ $/smdiv$
Sweep		$500ns$ $/smdiv$

Figure 4-23: Step and Impulse Response of the Overall System
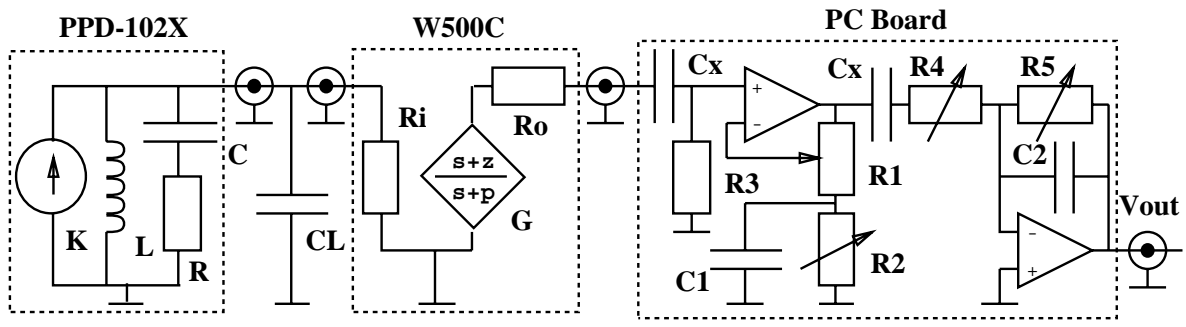
$$K = 1/3 = 0.33 \qquad C_L = 4.7nF \qquad C_1 = 2.0nF \qquad C_X = 0.1\mu F$$
$$L = 33\mu H \qquad R_L = R_i = 50\Omega \qquad R_1 = 5k\Omega(\text{pot.}) \qquad C_2 = 200pF$$
$$C = 3.6nF \qquad R_o = 50\Omega \qquad R_2 = 5k\Omega(\text{pot.}) \qquad R_4 = 1k\Omega(\text{pot.})$$
$$R = 100\Omega \qquad G = 42dB \qquad R_3 = 5.6k\Omega \qquad R_5 = 5k\Omega(\text{pot.})$$

Figure 4-24: Implemented Circuit Diagram of the Overall Implemented System
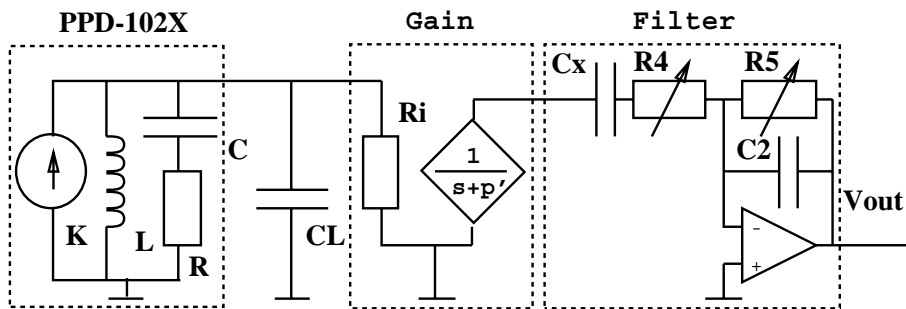
$$K = 1/3 = 0.33 \qquad C_L = 4.7nF \qquad C_X = 0.1\mu F$$
$$L = 33\mu H \qquad R_L = R_i = 50\Omega \qquad C_2 = 200pF$$
$$C = 3.6nF \qquad \qquad R_4 = 1k\Omega(\text{pot.})$$
$$R = 100\Omega \qquad \qquad R_5 = 5k\Omega(\text{pot.})$$

Figure 4-25: Generic Circuit Diagram of the Overall Implemented System
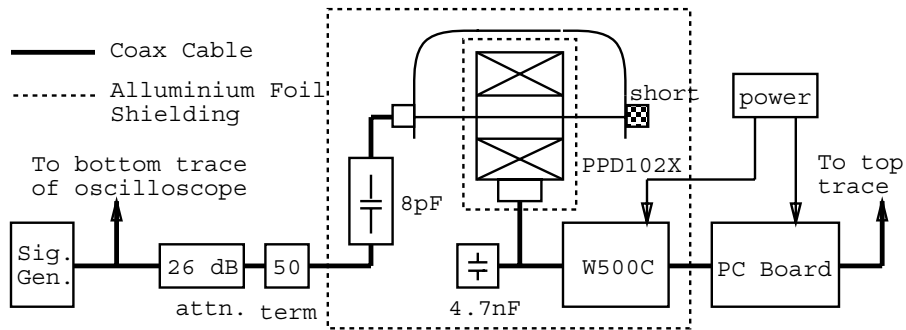
Figure 4-26: Experimental Setup for the Sensitivity Measurement

connected before the attenuators, because after the attenuation the signal is too low. The so attenuated step of voltage charges up the $8pF$ series capacitor and in doing so causes a small amount of charge to go through the current sensor. The output of the filter is registered by the top trace of the oscilloscope. Aluminium foil is used to shield the current sensor and other sensitive elements from external noise. All power connections are properly filtered locally using 10Ω series resistors and $0.1\mu F$ ceramic bypass capacitors.

The minimum pulse of current is shown on figure 4-27. The drive makes a $600mV$ step. Taking into account the $26dB$ attenuation, the area of the current pulse is:

$$Q = \frac{600mv}{40} \times 8pF = 120fC \tag{4.9}$$

As expected, this is a value approximately ten times larger than the calculated value of the MDS. (See equation 4.6.) A slower sweep rate was used in taking this picture, because it shows the thermal noise fluctuations more clearly. This experimental measurement confirms the expectations of the theoretical design.
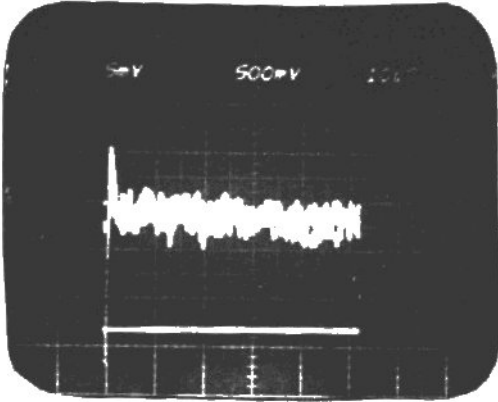
Trace	Description	Units
Top	Output (unloaded)	$5mV/smdiv$
Bottom	Drive before attn.	$5mV/smdiv$
Sweep		$10\mu s/smdiv$

Figure 4-27: Experimental Sensitivity Measurement

Chapter 5

Conclusions

In this thesis I design an analog system, which responds with an appropriate waveform to a pulse of current on the power line. My design uses limited resources in terms of what kind of current sensors and preamplifiers are available. I try to achieve the best performance with these resources.

The design developed in this work meets all specifications stated in the introduction. The measured sensitivity of the system, discussed at the end of Chapter 4, indicated that a charge of $120fC$ is well distinguishable against the background noise. This experimental value agrees very well with the theoretically calculated minimum detectable signal of $11.2fC$. The design aims at the best attainable signal-to-noise ratio and both the theoretical and experimental data confirm that the sensitivity of the system is adequate, knowing that partial discharges are in the picocoulomb range.

The experimental measurement of the impulse response follows the theoretical predictions. The waveform satisfies all requirements imposed by the digitizer. Its efficiency ($E = 0.136$), as defined in the introduction, is the highest out of the bipolar wave shapes presented in this work. It is lower than that of the perfect gaussian, but the latter lies entirely above zero, whereas this system is purposefully chosen to possess a bipolar response.[1]

The pole-zero configuration is centered around a dominant pole at -1.14×10^6,

---

[1] The response must integrate to zero. See Chapter 1.

allowing for a repetition rate of $220kHz$. This also meets the specifications.

The zero at the origin, introduced by the inductive coupling of the current sensor to the line, acts to reject lower frequencies. This is a quality of the transfer function which aids in the elimination of external noise, especialy $60Hz$ and harmonics.

Although there are many ways in which this design may be improved, it does meet the goals of the work. The experimental testing confirms the theory. The performance of the physically implemented system is at the expected level.

Appendix A

Software and Hardware Tools

A.1 *Software*

CLASCON   "CLASCON", (Classical Control Systems Analysis), is a program designed to analyze classical control systems. It focuses on analyzing feedback control systems. The program requires the definition of the open loop transfer function, determined by its pole-zero configuration and Bode gain. The program is capable of performing time-domain and frequency-domain analyses on the open-loop and the closed-loop systems.

I this thesis work I use this program to calculate the time-domain impulse and step responses of systems characterized by their pole-zero configurations. I also use it to calculate Bode data for such systems. All figures showing calculated step and impulse responses of various systems have been created with the help of CLASCON.

MAPLE   "Maple" performs numerical and symbolic computations in addition to having extensive graphics capabilities. I use this program to plot the functions shown on figure 1-3 and 1-1.

Other Software   Other software tools used in creating graphs and figures, and in general formatting include ProChart, IDraw, Xim, LaTeX.

A.2 *Hardware*

The oscilloscope I use is Tektronix 7633, with modules 7A16A, 7A26, 7B10. The photographs are taken on 667 Polaroid film.

The signal generator is ORTEC 419 Precision Pulse Generator. It has built-in attenuation and a 50Ω-output.

All coaxial cable is RG223/U, with a line impedance of 50Ω. I use 50Ω terminations and attenuators meant for use with 50Ω coaxial lines and many BNC connectors, angles, T-junctions.

The power supply used to power the W500C preamplifier and the custom-made printed circuit board is Global Specialties, 1310.

Bibliography

[1] Chathan M. Cooke. In-service power apparatus diagnosis by pulse partial discharge measurement and analysis: Background information. Technical Report Memo TM-90401, Massachusetts Institute of Technology, November 1990.

[2] C. H. Nowlin and J. L. Blankenship. Elimination of undesirable undershoot in the operation and testing of nuclear pulse amplifiers. *The Review of Scientific Instruments*, December 1965.

[3] J. L. Blankenship and C. J. Borkowski. Elimination of undesirable undershoot in the operation and testing of nuclear pulse amplifiers. *IRE Trans. Nucl. Sci. NS-8, No.1*, 1961.

[4] *Model 575 Amplifier: Operating and Service Manual.*

[5] *Model 450 Research Amplifier: Operating and Service Manual.*

[6] *Model 113 Scintillation Preamplifier: Operating and Service Manual.*